THE MESOSCALE PREDICTABILITY EXPERIMENT (MPEX)

BY MORRIS L. WEISMAN, ROBERT J. TRAPP, GLEN S. ROMINE, CHRIS DAVIS, RYAN TORN, MICHAEL BALDWIN, LANCE BOSART, JOHN BROWN, MICHAEL CONIGLIO, DAVID DOWELL, A. CLARK EVANS, THOMAS J. GALARNEAU JR., JULIE HAGGERTY, TERRY HOCK, KEVIN MANNING, PAUL ROEBBER, PAVEL ROMASHKIN, RUSS SCHUMACHER, CRAIG S. SCHWARTZ, RYAN SOBASH, DAVID STENSRUD, AND STANLEY B. TRIER

The MPEX field campaign incorporates enhanced mesoscale observations of the upstream and nearby convective environment to improve the predictability of convective events.

Explicit predictions of convective weather with numerical models that assimilate high-resolution observations are recognized as essential for improving warnings of hazardous weather associated with convective storms (tornadoes, other damaging winds, hail, lightning, and floods) and improving quantitative precipitation forecasts in general (Fritsch et al. 1998; Droegemeier et al. 2000; Dabberdt et al. 2000). Additionally, various real-time experiments during the last decade have demonstrated that explicit prediction of convective storms (Lilly 1990; Droegemeier 1990, 1997) has now become a reality (e.g., Droegemeier et al. 1996; Xue and Martin 2006a,b; Done et al. 2004; Kain et al. 2005, 2006, 2008; Weisman et al. 2008; Lean et al. 2008; Rotach et al. 2009; Seity et al. 2011; Clark et al. 2012). However, it is an open question whether current operational analyses are sufficiently accurate to maximize the potential predictability of convective events using such convection-permitting models.

Theoretical studies clearly suggest that the predictability of weather phenomena decreases with decreasing scale, ranging from several days for synoptic-scale disturbances, down to mere hours for convective storms (e.g., Lilly 1990). Moreover, most data assimilation studies to date suggest that the value of adding convective-scale details to the initial forecast state, via the direct incorporation of radar data or the indirect use of diabatic heating to represent ongoing convection, is no longer discernible after the first 6–8 h of a forecast (e.g., Kain et al. 2010a; Sun et al. 2012; Stratman et al. 2013). However, to the degree that convective storms are forced and constrained by larger-scale phenomena such as fronts, drylines, and jet streaks or the degree to which convection produces significant modifications to its regional environment, improving the representation of these forcing elements and convective feedbacks has the potential to significantly improve the predictability of the convective weather as well.

With this in mind, the experimental plan for the Mesoscale Predictability Experiment (MPEX) was guided by the following two scientific hypotheses:

1) Enhanced synoptic and subsynoptic-scale observations over the Rocky Mountain region (e.g., Colorado, New Mexico, Arizona, Utah, and Wyoming) during the early morning will significantly improve the forecast of the timing and location of convective initiation as well as convective evolution during the afternoon and evening over the high plains.

2) Enhanced subsynoptic-scale observations in the late afternoon, over regions where the atmosphere is being convectively disturbed, will significantly improve the 0–24-h forecast of convective and synoptic-scale evolution in downstream regions.

The scientific basis for each of these hypotheses is described in more detail in the sections below.

Regional analysis and numerical weather prediction. Since 2003, experimental daily 24–48-h, real-time, explicit convective forecasts employing horizontal grid spacings between 1 and 4 km over the central United States have been evaluated as part of the NOAA Hazardous Weather Testbed (HWT) Spring Forecasting Experiments, wherein forecasters and researchers from a variety of backgrounds have evaluated the application of such high-resolution guidance for operational severe storm forecasting (e.g., Weiss et al. 2004, 2007; Kain et al. 2005, 2006, 2008; Clark et al. 2012; Kain et al. 2013). These forecast exercises have demonstrated that increasing horizontal grid resolutions into the convective-allowing regime leads to significant improvements in convective forecast guidance. For instance, such forecasts often realistically represent the structure and evolution of mesoscale convective phenomena, such as supercells, squall lines, bow echoes, and mesoscale convective vortices as well as the convective diurnal cycle, yet significant errors in the timing and location of convective events are also sometimes encountered (e.g., Done et al. 2004; Kain et al. 2008; Hohenegger and Schär 2007; Weisman et al. 2008; Snively and Gallus 2014).

Numerous issues could contribute to these forecast errors, including errors in physical parameterization schemes (e.g., Kain et al. 2005; Weisman et al. 2008; Coniglio et al. 2013), coarse horizontal and vertical resolution (e.g., Kain et al. 2008; Schwartz et al. 2009; Vandenberg et al. 2014), and poor representation of atmospheric features crucial to storm initiation and evolution (e.g., Coniglio et al. 2010; Duda and Gallus 2013). While studies considering variations in grid resolution and/or model physics [e.g., planetary boundary layer (PBL) and microphysics] do show sensitivity in the details of storm structure and evolution, they have generally not been able to explain the larger, mesoscale forecast errors that are often observed. However, far more forecast sensitivity on the 6–48-h time scale is often found by varying initial conditions [e.g., initializing with the National Centers for Environmental Prediction (NCEP) North American Mesoscale (NAM) versus Global Forecast Systems (GFS) analyses], providing a larger spread of possible outcomes that seems to offer a better chance of encompassing the correct forecast (e.g., Weisman et al. 2008; Clark et al. 2010a,b).

An example of the range of solutions that often results from using differing analysis schemes is presented in Fig. 1 from 15 May 2013 during the MPEX field campaign. In this example, 12-h forecasts initialized at 1200 UTC with an identically configured Weather Research and Forecasting (WRF) Model using a 3-km horizontal grid (as described in the section on "Real-time ensemble modeling and sensitivity analysis") are compared. These forecasts are initialized using GFS, NAM, and a representative member of an ensemble Kalman filter (EnKF) analysis system (as also described in the section on "Real-time ensemble modeling and sensitivity analysis"). A fairly wide spectrum of forecast convective outcomes is noted, ranging from a well-organized isolated bow echo in northeast Texas using the EnKF analysis to more widespread clusters of convection in Texas and Oklahoma using the NAM and GFS analyses. Unfortunately, none of these forecasts closely matches the observed radar composite at 0000 UTC, which depicts a primary bow-shaped convective system in south-central Oklahoma, with more isolated convective cells extending southward into the Dallas–Ft. Worth, Texas, region. Several of these cells in the Dallas–Ft. Worth region were supercellular, producing a series of significant tornadoes that were not well anticipated by operational forecasters based on the early morning guidance.

Such examples suggest that current analysis capabilities at the subsynoptic and mesoscale may, at

AFFILIATIONS: Weisman, Romine, Davis, Galarneau, Haggerty, Hock, Manning, Romashkin, Schwartz, Sobash, and Trier—National Center for Atmospheric Research, Boulder, Colorado; Trapp—University of Illinois at Urbana–Champaign, Urbana, Illinois; Torn and Bosart—University at Albany, State University of New York, Albany, New York; Baldwin—Purdue University, West Lafayette, Indiana; Brown and Dowell—NOAA/ESRL, Boulder, Colorado; Coniglio—NOAA/NSSL, Norman, Oklahoma; Evans and Roebber—University of Wisconsin–Milwaukee, Milwaukee, Wisconsin; Schumacher—Colorado State University, Ft. Collins, Colorado; Stensrud—The Pennsylvania State University, University Park, Pennsylvania
CORRESPONDING AUTHOR: Morris L. Weisman, NCAR, P.O. Box 3000, Boulder, CO 80307
E-mail: weisman@ucar.edu

The abstract for this article can be found in this issue, following the table of contents.
DOI:10.1175/BAMS-D-13-00281.1

In final form 12 December 2014

times, limit the forecast skill for significant convective events. One of the major goals of MPEX is, thus, to better document the current limitations of the operational analysis systems and to test whether convective forecasting could be improved through the enhancement of observation density for features of interest using the dropsonde, upsonde, and microwave temperature profiler (MTP) data collected during the field campaign. The potential benefits of the enhanced observations for analysis and prediction are being tested using a variety of different methods, as are described in the sections below on "Real-time ensemble modeling and sensitivity analysis" and "Research plans and opportunities."

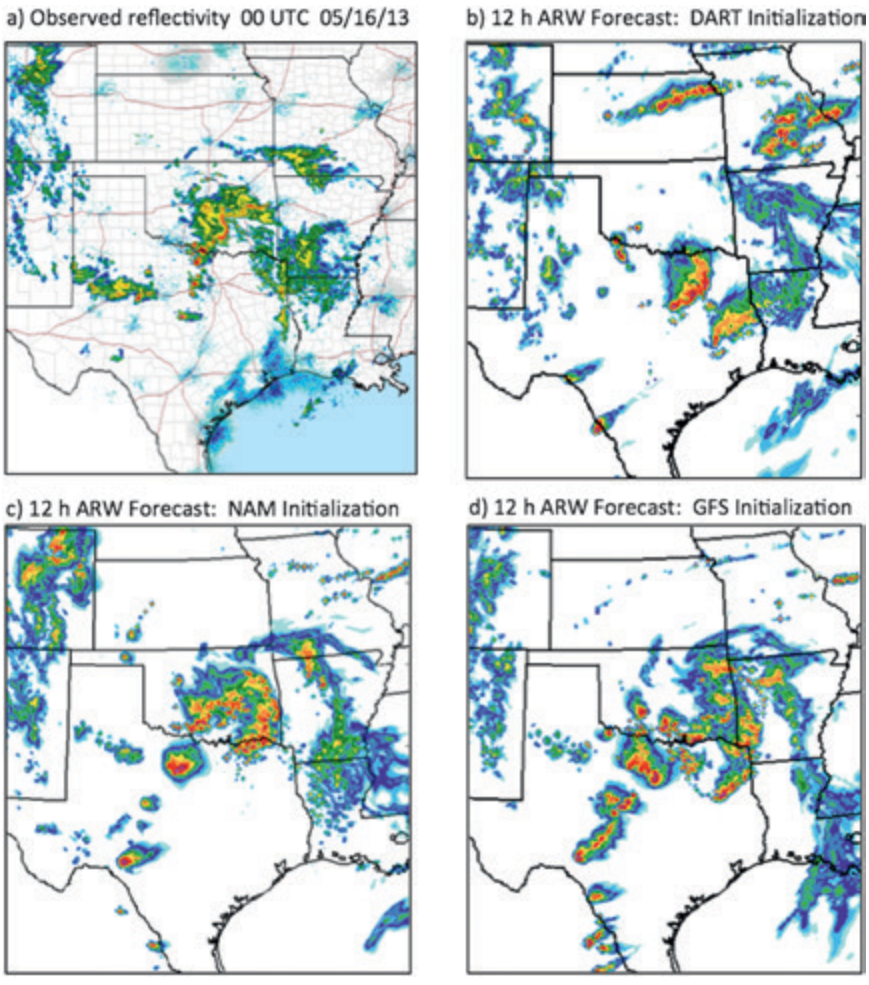

Fig. 1. (a) Observed composite reflectivity at 0000 UTC 16 May 2013, as compared with 12-h reflectivity forecasts using the Advanced Research version of WRF (ARW) with a 3-km grid spacing, initialized at 1200 UTC 15 May using (b) a representative analysis from the DART ensemble, as described in the text; (c) the analysis from the operational NAM model; and (d) the analysis from the operational GFS model.

Storm–environment feedbacks. The influence of organized regions of deep convection on the large-scale environment in both space and time has been recognized for many years. Upper-tropospheric meso-α-scale anticyclones commonly are associated with cloud clusters, tropical storms, and hurricanes in the tropics (Riehl 1959; Yanai 1964; Houze and Betts 1981) and mesoscale convective systems (MCSs) in the midlatitudes (Ninomiya 1971a,b; Maddox 1980; Fritsch and Maddox 1981; Anabor et al. 2009; Trier and Sharman 2009; Metz and Bosart 2010). These anticyclones can have significant amplitudes, with perturbations in wind speeds of over 20 m s^{-1} and in geopotential heights of over 80 m at 200 hPa (Leary 1979; Fritsch and Maddox 1981; Perkey and Maddox 1985; Smull and Augustine 1993). They typically develop during the mature stage of a convective system and dissipate during the decay stage (Houze 1977; Leary 1979; Gamache and Houze 1982; Wetzel et al. 1983; Menard and Fritsch 1989). This yields a relatively short lifetime of approximately 6–24 h within which to sample these features produced by storm–environment interactions.

Further evidence of the ability of midlatitude MCSs to produce longer-lived effects on the environment is given by Keyser and Johnson (1984) and Wolf and Johnson (1995a,b), who illustrate the ability of organized deep convective regions to enhance upper-level jet streaks through modification of the direct mass circulation in jet entrance regions by diabatic heating. Stensrud (1996) and Stensrud and Anderson (2001) further show that long-lived regions of deep convection can act as a Rossby wave source region and produce significant upper-level perturbations to the large-scale flow. Long-lived regions of deep convection also tend to increase the low-level inflow

of warm, moist air that helps sustain the convection (Stensrud 1996).

On the smaller scale, closer to the region of deep convection in both space and time, Brooks et al. (1994) show changes in the convective available potential energy (CAPE) and storm-relative environmental helicity surrounding a simulated supercell thunderstorm. The supercell enhances both CAPE and helicity in the inflow region within 2 h after initiation, with changes extending 10–20 km out from the storm core. These changes likely assist supercell maintenance and may increase storm severity. Similar environmental modifications are noted by Parker (2014) based on near-storm soundings taken during the second Verification of the Origins of Rotation in Tornadoes Experiment (VORTEX2) field campaign. Thus, even isolated, short-lived thunderstorms influence the nearby environment.

While these past studies clearly document the influences of thunderstorms and MCSs on the environment in which they are embedded, both near the convection and more distant, a careful comparison of the upscale response to convection found in model simulations with the environmental observations has not been conducted. With the improved capability of numerical weather prediction (NWP) models at convection-allowing grid spacing (1–4 km), however, it is time to examine the details of how deep convection modifies the surrounding environment in much greater detail.

It is well known that the characteristics of convective storms are strongly tied to the environment in which they develop; thus, it is important to represent the initial environment accurately to be able to forecast convection accurately (Benjamin et al. 2010; Wandishin et al. 2010). For example, Stensrud and Gao (2010) show that a horizontally inhomogeneous background environment derived from an assimilation of surface observations significantly improves 1-h forecasts of a tornadic thunderstorm on 1–3-km grids over those provided by horizontally homogeneous initial conditions. For the successful prediction of a squall line on a 4-km grid, Sun and Zhang (2008) show that assimilation of wind observations from a nearby environmental sounding are very important. Schenkman et al. (2011) show that 1–2-h forecasts of an MCS on a 2-km grid and an embedded vortex are impacted positively and significantly by the assimilation of surface mesonet data. Although the abovementioned studies show the importance of representing the environment accurately for short-term convective forecasts, they are limited in scope, only considering single squall-line simulations and only incorporating limited operational data rather than the enhanced field data collected during MPEX. A careful examination of the impact of multiple radiosonde observations at mesoscale space and time scales on the short-term (0–24 h) prediction of convection has yet to be performed.

MODELING AND DEPLOYMENT STRATEGIES. A mission timeline (Fig. 2) helps to clarify the relative placement and roles of the modeling and observational assets employed during MPEX. As with other recent field efforts [e.g., Bow Echo and Mesoscale Convective Vortex Experiment (BAMEX) in Davis et al. (2004); VORTEX2 in Wurman et al. (2012); Deep Convective Clouds and Chemistry (DC3) in Barth et al. (2015)], operations and deployment planning was strongly guided by output from experimental high-resolution models, as described below in the section on "Real-time ensemble modeling and sensitivity analysis." Since a go or no-go decision for the next morning's flight operations needed to be made at the daily 2100 UTC briefing, the primary model forecast input to this planning came from the earlier 1200 UTC modeling suites, roughly 24 h ahead of the intended dropsonde and MTP operations and about 36 h ahead of the expected convective event. Initial decisions regarding any possible next-day upsonde operations were also discussed at the daily briefing, as operations allowed (e.g., if upsonde operations were not ongoing), with minor modifications considered based on model and observational updates through the evening and following morning.

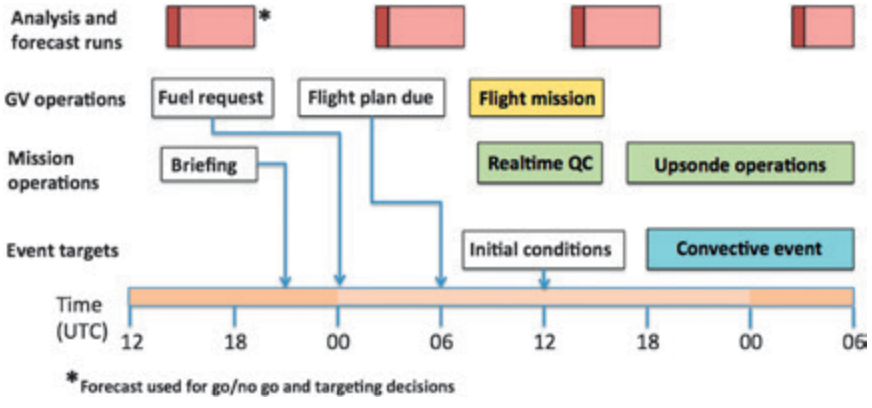

Fig. 2. Mission timeline.

National Science Foundation (NSF)–National

Center for Atmospheric Research (NCAR) Gulfstream V (GV) research flights generally extended from 0900 to 1500 UTC, targeting specific regions thought to be especially significant for later-in-the-day convective activity (generally occurring from 1800 to 0600 UTC). Upsonde teams then positioned themselves in the late morning through early afternoon period to sample the pre- through post-convective environments of their specified targeted regions. More specific details concerning these modeling and operational assets and deployment strategies are offered in the sections below.

Real-time ensemble modeling and sensitivity analysis. Five research model configurations were used in MPEX in addition to the operational models to make weather forecasts and judge forecast uncertainty (Table 1). The primary research guidance was from an experimental 3-km WRF Model (Skamarock et al. 2008) initialized from an NCAR-generated 50-member ensemble analysis system based on WRF–Data Assimilation Research Testbed (DART) (Anderson et al. 2009). DART is an ensemble-based data assimilation system that provides interfaces to a number of models. Used as a cycled data assimilation system, DART provides periodic analysis and initial conditions for deterministic or probabilistic forecasts. Further, diagnostics generated by DART provide key feedback on model system deficiencies in representing observed features.

For MPEX, each ensemble member forecast included a contiguous United States (CONUS) mesoscale (15 km) and two-thirds CONUS nest (3 km; extending from roughly Utah to West Virginia), with forecast products based on the explicit nest. The 30-member ensemble forecasts extending through 48 h were produced twice daily (initialized from the 0000 and 1200 UTC WRF–DART analyses) on the NCAR Yellowstone supercomputer.

The real-time WRF ensemble forecasts generated during this period were also used to objectively determine the locations and variables where errors would have the greatest impact on subsequent forecasts of convection using the ensemble-based sensitivity analysis (ESA) technique (Ancell and Hakim 2007; Torn and Hakim 2008). Here, sensitivity is defined as the change in a forecast metric at some particular lead time (i.e., 36-h precipitation averaged over a particular region) per unit change in an individual model state variable at an earlier lead time (i.e., 24-h wind, temperature, or moisture at a location). Locations where the magnitude of the sensitivity is relatively large suggest locations where errors can grow most rapidly and impact the forecast metric; therefore, it provides an assessment for where assimilating additional observations could improve a forecast should an error already exist. Although sensitivity analysis has been used for observation targeting in both midlatitude (i.e., Joly et al. 1999; Szunyogh et al. 2000) and tropical cyclone applications (Aberson 2003; Wu et al. 2007), MPEX represented the first time that sensitivity analysis has been used for mesoscale observation targeting. Moreover, sensitivity analysis provides a quantitative method of testing hypotheses

Table 1. Summary of high-resolution modeling tools employed during MPEX. Mountain daylight time (MDT) is UTC minus 6 h.

Name	Run time	Update time	Time available to community	Initialization approach
3-km NCAR ARW ensemble forecasts	Two 48-h simulations run daily	0000 UTC 1200 UTC	0000 MDT 1200 MDT	Cycling WRF–DART analyses
3-km ARW ensemble sensitivity analyses	Based on 1200 UTC 3-km ARW	1200 UTC	1300 MDT	—
4-km WRF NSSL weather forecasts	Two 36-h simulations run daily	0000 UTC 1200 UTC	2300 MDT 1100 MDT	NAM analyses
3-km HRRR forecasts	15-h forecasts	Hourly	Analysis time plus 2 h	RAP analyses
CSU 4-km WRF forecasts	39-h forecasts	1200 UTC	1500 MDT	GFS analyses

about what features (i.e., troughs and dryline) or fields (i.e., boundary layer moisture and CAPE) contribute to changes in the subsequent forecast.

During MPEX, forecast sensitivities were computed for multiple forecast metrics using the WRF ensemble forecasts, which in turn were used as guidance for planning GV missions. For each set of forecasts initialized at 1200 UTC, multiple boxes were defined based on locations and time periods where the 3-h precipitation standard deviation and vertical motion was large between 2100 and 0300 UTC during the next day. From the list of potential metric boxes, one or two boxes were subjectively chosen as a basis for a mission based on convective type and coordination with upsonde operations. Maps of sensitivity of the precipitation to individual grid points were overlaid on the particular field valid at 1200 UTC the next day (i.e., centered on the GV mission time) to scrutinize the relationship between the sensitivity pattern and the features that were believed to be important to the forecast, such as the position of midtropospheric troughs and moisture, surface boundaries, and so on. In situations where the regions of large sensitivity lined up with the features that were subjectively believed to be important to the forecast, GV flight patterns were designed that would sample the feature and the sensitive region.

Additional daily explicit (4 km) WRF deterministic model forecasts were supplied by Colorado State University (CSU) and the National Severe Storms Laboratory (NSSL), based on GFS and NAM initial conditions, respectively, allowing for valuable intercomparisons with the WRF–DART ensemble forecasts. Finally, the dropsonde data were assimilated into real-time models by the Assimilation and Modeling Branch of the Global Systems Division at the National Oceanic and Atmospheric Administration (NOAA)'s Earth System Research Laboratory. Parallel, experimental versions of the Rapid Refresh (a 13-km WRF system; Ikeda et al. 2013; Zhu et al. 2013) and High-Resolution Rapid Refresh (a 3-km WRF system; Ikeda et al. 2013) were run, both with and without dropsonde data assimilation. Forecast output was available in real time during the second half of the field experiment, and forecasts for earlier cases have since been produced retrospectively.

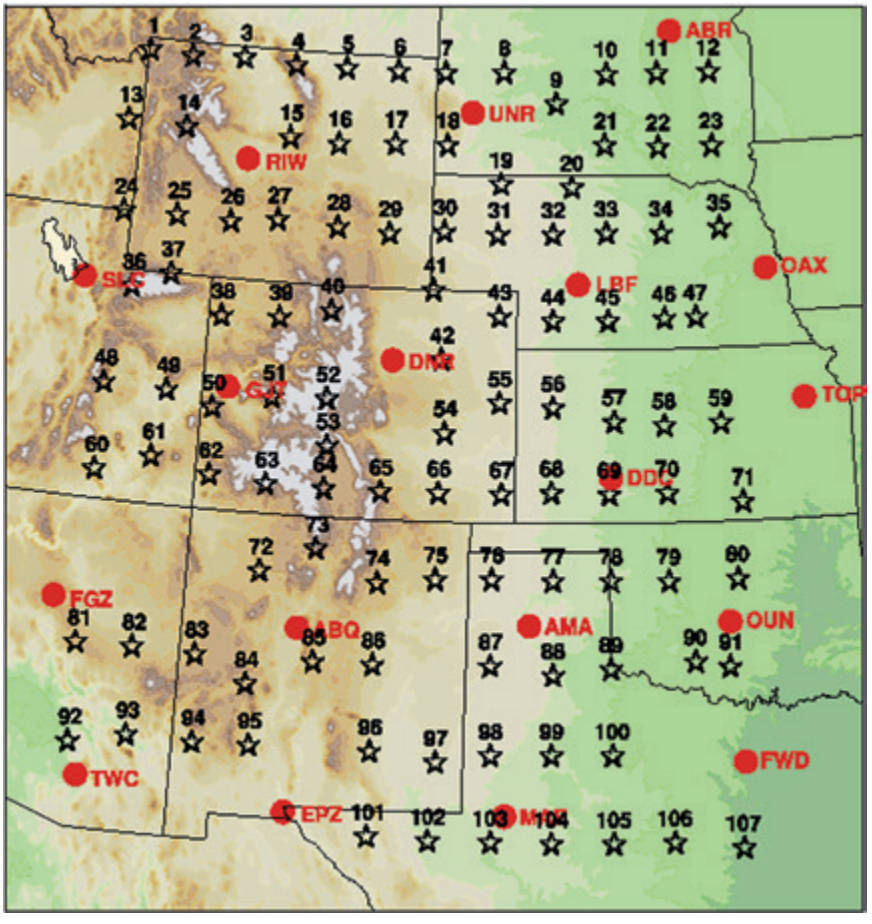

Fig. 3. Full domain of interest for MPEX morning dropsonde operations, along with a prevetted set of dropsonde sites (numbered stars). Operational NWS sounding sites are indicated by the red dots.

Morning dropsonde and MTP strategies. The goal for the morning dropsonde deployments was to obtain wind, temperature, and moisture observations through the depth of the troposphere on a grid that was sufficiently dense to sample subsynoptic shortwave troughs and ridges, low-level jets, dry intrusions, potential vorticity streamers, and other mesoscale phenomena in the prestorm environment (typical sample spacing was about 75–200 km). GPS mini dropsondes deployed from the GV aircraft (see sidebar on "The NCAR GV and mini dropsonde system") were

THE NCAR GV AND MINI DROPSONDE SYSTEM

The NSF–NCAR GV Airborne Vertical Atmospheric Profiling System (Hock and Franklin 1999; Fig. SB1) is an atmospheric instrument that measures vertical profiles of ambient temperature, pressure, humidity, wind speed, and wind direction. Measurements are taken by a parachuted dropsonde that is launched from the aircraft and descends to the surface. In situ data collected from the sonde's sensors are transmitted in real time to an onboard aircraft data system via radio link. Up to eight dropsondes can be tracked in the air simultaneously.

The dropsonde is composed of a small electronic circuit board, sensors, and a battery housed in a cardboard tube with a parachute. The total weight of the sonde is less than 6 oz (<170 g) with dimensions of a 1.75-in.-diameter tube 12 in. long (1 in. = 2.54 cm). The inner electronic components of the dropsonde consist of precision temperature, pressure, and humidity sensors; a telemetry transmitter; and a GPS receiver for winds and microprocessors. As the sonde descends, it continuously measures the atmosphere from the release altitude to Earth's surface. Measurements are made every half second for the thermodynamic data and every 0.25 s for winds, which provides a precise detailed profile of the atmosphere. The parachute deploys from the top of the sonde within seconds of being released from the aircraft. The parachute is specially designed for high reliability and a very stable descent. The fall velocity of the dropsonde varies with air density, ranging from ~22 m s^{-1} at 200 hPa to ~12 m s^{-1} at 875 hPa during the MPEX missions. As the sonde descends, the GPS receiver tracks the position and velocity of the sondes; this change in motion corresponds to the atmospheric winds. Once the sounding is complete, the data are automatically sent to the ground via the GV satellite system for quality-control processing, creating skew-*T* plots and World Meteorological Organization (WMO) TEMP DROP messages. MPEX was the first deployment of the NCAR mini dropsonde from the GV using a newly developed automated dropsonde launch system.

The pressure, temperature, and humidity sensor used in the sonde is a Vaisala sensor module, which is almost identical to that used in the RS-92 radiosonde. These sensors were chosen for their performance characteristics of accuracy, range, response time, and minimal impact by solar radiation. Each sensor module is individually calibrated for high accuracy.

Fig. SB1. The NCAR NSF GV aircraft and new mini dropsonde.

successfully used for this task, representing the first official use of the new mini dropsondes being deployed from an automatic launch system from the GV. An airborne MTP (e.g., Haggerty et al. 2014) was also deployed on the GV (see sidebar on "The microwave temperature profiler") and offered a continuous vertical profile of atmospheric temperature (or potential temperature), extending roughly 6 km above and below the aircraft's altitude along the aircraft's path. As such, MTP data significantly enhanced the characterization of the atmospheric structure between dropsondes, thereby increasing the effective resolution of the observational dataset even further.

The full GV observational domain for MPEX is depicted in Fig. 3. Within this domain, potential drop sites were prevetted to avoid no-drop zones based on population, military, or air traffic flow constraints. Also, drop sites were chosen so as to not overlap with existing National Weather Service (NWS) sites to maximize the value added by the deployment strategy. A flight altitude of at least 12 km (40,000 ft) was used for all drops to allow for the sampling of deep-layer shear, stability, and moisture as well as to characterize upper-/midtropospheric features that may be important for subsequent convective initiation.

A subdomain of roughly 600 km × 1,000 km was typically chosen for each 1-day intensive observing

MTP (Haggerty et al. 2014) is a scanning radiometer that provides measurements related to atmospheric temperature structure above and below the aircraft. Basic components of the MTP are a receiver that measures emission centered on three lines within the oxygen absorption complex and a scanning mirror that views emission at 10 elevation angles between nadir and zenith. Profiles are produced every 17 s or about every 4 km along the flight path. A statistical retrieval algorithm using historical radiosonde profiles is applied to convert the observed brightness temperature into temperature as a function of altitude.

An example from 19 May 2013 is shown in Fig. SB2. Figure SB2 (bottom left) shows the segment of the GV mission that transected the upper-tropospheric front over northern New Mexico. In Fig. SB2 (top), the front is seen as a fold in the 2 potential vorticity unit (PVU; 1 PVU = 10^{-6} K kg^{-1} m^2 s^{-1}) surface of potential vorticity as depicted by the National Centers for Environmental Prediction GFS analysis at 1200 UTC 19 May (purple). Temperature anomalies derived from the MTP

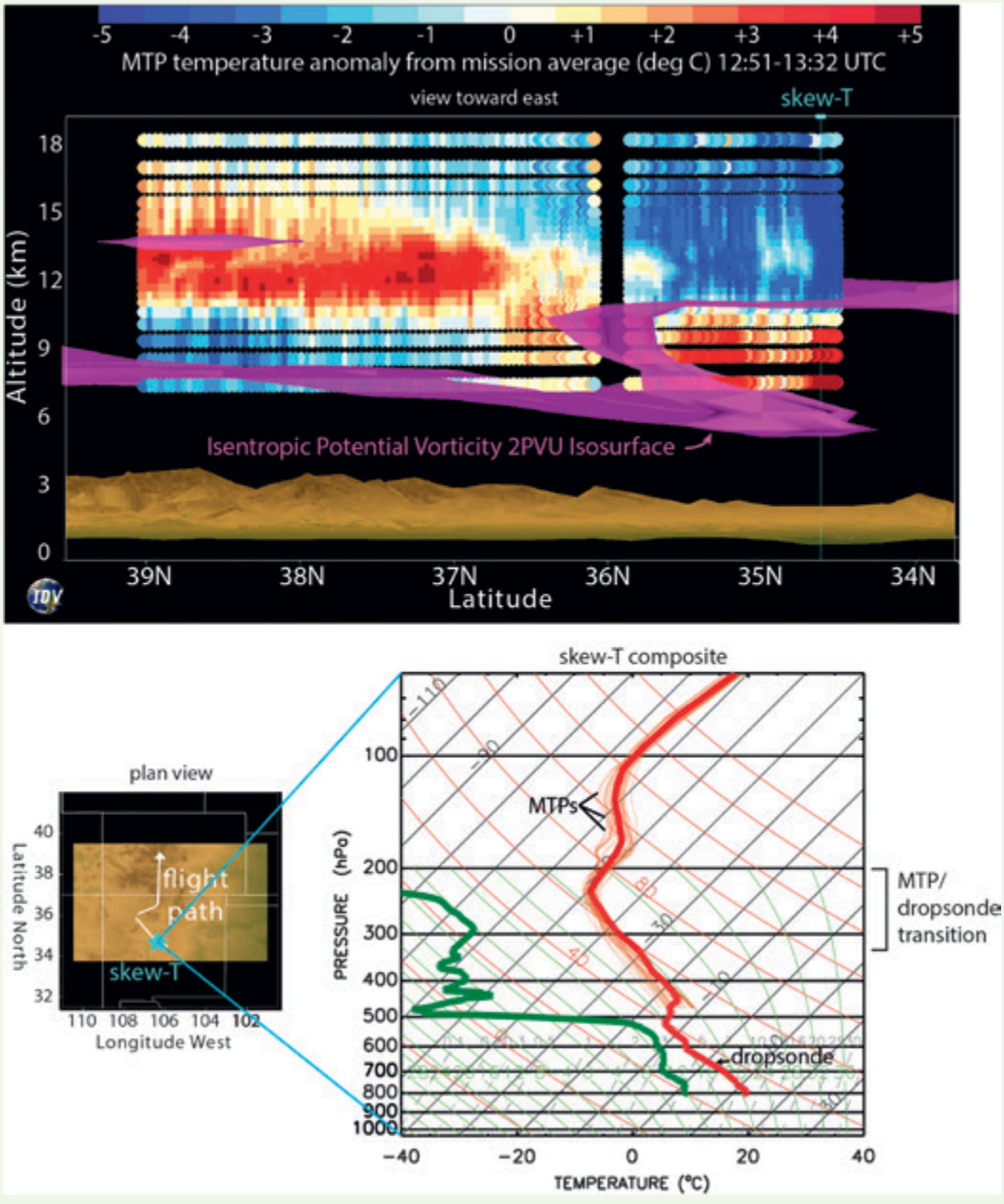

Fig. SB2. Sample MTP temperature cross section and MTP–dropsonde-derived composite sounding, as described in the text.

are shaded from blue (negative) to red (positive), where the anomaly is defined relative to the mission average temperature at each altitude. The reversal of the meridional temperature gradient from troposphere to stratosphere is clearly seen, as is the weakening of the temperature gradient where the tropopause becomes vertical in the jet core near 36°N. In Fig. SB2 (bottom right), a deep temperature sounding through the upper-level frontal zone [see the light blue vertical line marked "skew-*T*" in Fig. SB2 (top)] is constructed by superposing a weighted average of dropsonde temperatures and the mean of MTP profiles over a 5-min period (temperature in red, dewpoint in green). The composite sounding reveals three isothermal layers, one near 500 hPa (the upper-level front), another near 200 hPa (the nominal tropopause), and a third well into the stratosphere above 100 hPa.

period (IOP) depending on the meteorological scenario. Within the specified subdomain, 28–34 sondes were dropped per IOP, with the drop spacing ranging between 75 and 250 km, focused on the targeted subsynoptic feature of interest. An example flight path is presented in Fig. 4 for 31 May 2013, where dropsondes characterized the environment in the morning upstream from Oklahoma, prior to a significant tornado and flood event in central Oklahoma later that day.

Dropsonde and MTP deployments occurred on days for which widespread (severe) convection (preferably with an identifiable upstream precursor) was forecast, based on operational and experimental convection-allowing forecast guidance and especially if significant uncertainty was noted in the model or human forecast guidance. In the present context, forecast uncertainty reflected uncertainty in the timing, location, or intensity of potential convection. "Uncertainty" was measured via the apparent level of disagreement between the various operational and experimental models and/or human forecasters as well as from the more formal sensitivity analyses produced from the WRF–DART high-resolution ensemble, as described in the section above on "Real-time ensemble modeling and sensitivity analysis."

Afternoon upsonde strategies. GPS upsondes (i.e., balloonborne radiosondes) were deployed during specific afternoons and evenings to characterize the mesoscale environment over regions of anticipated convection initiation (CI) as well as the mesoscale environment that had been disturbed by subsequent convective storms. Two dual-frequency radiosonde systems operated by Purdue University and NSSL, and an additional single-frequency radiosonde system operated by CSU (see the appendix for system details) were used. Combined, these systems allowed up to five sondes to be in the air simultaneously. For one week in late May, a fourth mobile system was contributed by Texas A&M University (TAMU) and thus allowed for simultaneous sampling with six sondes.

Several different deployment strategies were employed by the upsonde teams. For instance, a preconvective environment (PCE) strategy (Fig. 5) could be conducted to sample the full tropospheric structure of the mesoscale environment, prior to and in the region of anticipated CI. Starting with about 60–80-km, north–south separation between two of the teams, the basic plan was for both teams to simultaneously release a radiosonde, redeploy roughly 80 km downstream, and then each simultaneously release a second radiosonde; a third team would follow a similar strategy, except with about 20-km redeployment distance. The three radiosonde teams were positioned relative to the time and location of expected CI, with the first radiosonde observations made upstream of the expected CI location and the last observations made downstream, when CI occurs. Logistics permitting, locations for

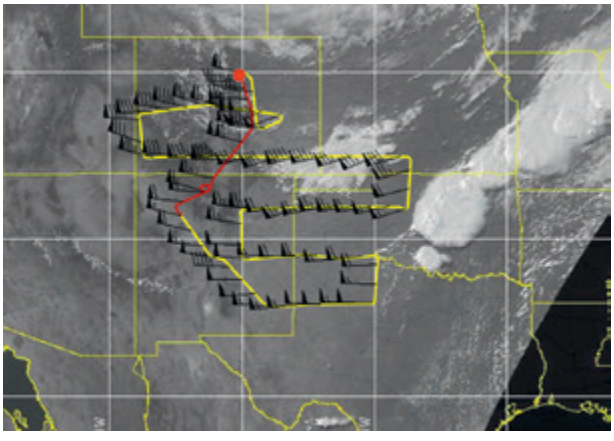

Fig. 4. Example of upstream GV deployment (yellow) for the early morning of 31 May 2013 (~0900–1500 UTC), showing airflight winds at ~40,000 ft MSL. The visible satellite background is at 0000 UTC 1 Jun, depicting the resulting severe convective outbreak extending from central Oklahoma northeastward through Missouri. The red GV flight track signifies the last hour of the flight.

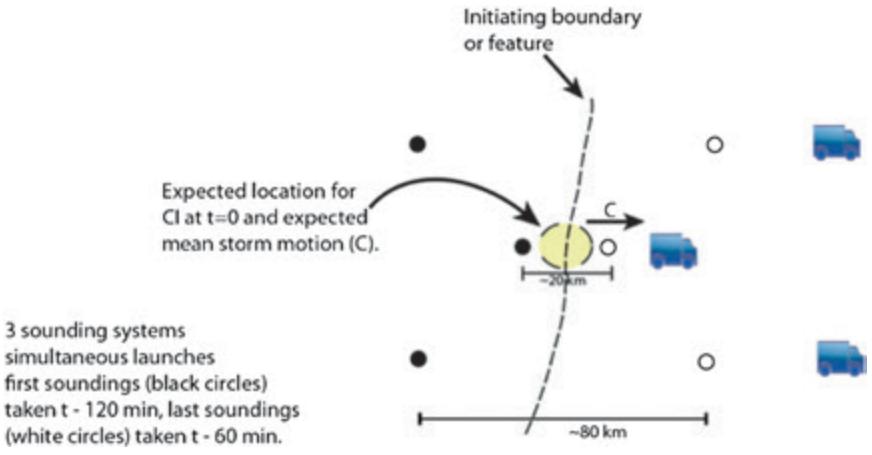

Fig. 5. Example of upsonde locations (circles) for the PCE sampling strategy.

the PCE deployments were generally chosen to be downwind of the morning observational domain that was sampled by the GV and in regions thought to be observationally sensitive, based on the ESA.

Similarly, the goal of the convectively disturbed environment (CDE) strategy was to sample the mesoscale environment that has been disturbed by the subsequent convective storms. Starting with approximately 2*D*–3*D* north–south separation, the basic plan (Fig. 6) given offset distance *D* was to execute time-coordinated releases of a series of radiosondes at fixed locations, at 0.5–1-h intervals. The radiosonde teams were positioned relative to the convective storm motion ***C***, such that the first (last) radiosonde observations would be made in advance of (in the wake of) the moving storm. Distance *D* depended on the availability of suitable radiosonde release locations but nominally was between 5 and 25 km.

MPEX IOP SUMMARY AND CASE EXAMPLES. The weather pattern experienced during MPEX was quite active, offering a wide spectrum of opportunities to sample convective environments, ranging from weakly forced convective events to several strongly forced severe weather outbreaks, including destructive tornadic events impacting Grandbury, Texas (May 15); Moore, Oklahoma (May 20); and El Reno, Oklahoma (May 31). In all, 15 morning missions were successfully completed with the GV, with 17 afternoon missions completed with the mobile soundings units (including all but one of the GV days plus three additional days when the GV was unavailable because of the duty cycle limitations). A total of 18 IOPs is listed in Table 2, along with a brief meteorological description and notes on the number of dropsondes and upsondes that were deployed for each case. A few examples of the range of morning dropsonde deployments during MPEX are presented in Fig. 7, representing a weak, upper-level closed low in the Texas Panhandle (15 May); a weak disturbance in southwesterly flow over New Mexico (28 May); a strong jet stream and upper-tropospheric front centered over southern Colorado and northern New Mexico (30 May); and an upper-level short wave and associated cold front in northwesterly flow centered over Wyoming (8 June). Afternoon upsonde missions included the sampling of a pair of supercells and their transition to a quasi-linear convective system (QLCS) in the southern Texas Panhandle (23 May), a damaging QLCS and its northern bookend vortex in the Texas Panhandle (29 May), a large tornadic supercell in central Oklahoma (31 May), and a supercell-to-bow-echo transition in the Oklahoma Panhandle (3 June; see Fig. 8).

A more detailed case example from 19 May 2013, which was representative and well sampled with both the GV and upsonde teams, helps illustrate the

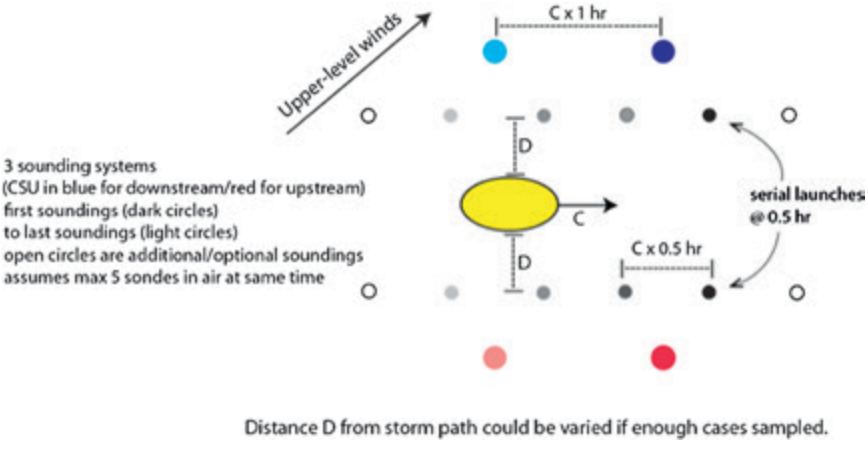

Fig. 6. Example of upsonde locations (circles) for the CDE sampling strategy. The open circles represent additional/optional soundings that can be made if time allows.

experimental process followed during MPEX. The synoptic pattern for this day was dominated by a deep and broad 500-hPa trough over the Rocky Mountains, with a strong jet stream and a mid- to-upper-tropospheric front extending from Nevada through Arizona and New Mexico and northeastward through Texas, Oklahoma, Kansas, and Missouri (Fig. 9a). A surface cold front was situated from northeastern South Dakota southward through Nebraska and western Kansas, with a dryline extending from a weak, low pressure center in southwestern Kansas southward through the Texas Panhandle and southwestern Texas (Fig. 9a). The satellite water vapor image at 1200 UTC (Fig. 9b) depicts a fairly moist environment in the mid- to upper troposphere from Kansas northward, with the remains of nocturnal MCSs evident in eastern Kansas as well as farther northeast into Illinois and Wisconsin. Ahead of the cold front and dryline, the environment was characterized by high CAPE and strong vertical wind shear, and a significant severe weather outbreak (including tornadoes) was anticipated by Storm Prediction Center (SPC) forecasters across a broad region from north-central Oklahoma northward into central and eastern Kansas and Missouri.

Forecasts from the ensemble initialized at 1200 UTC 18 May suggested two concentrated regions where

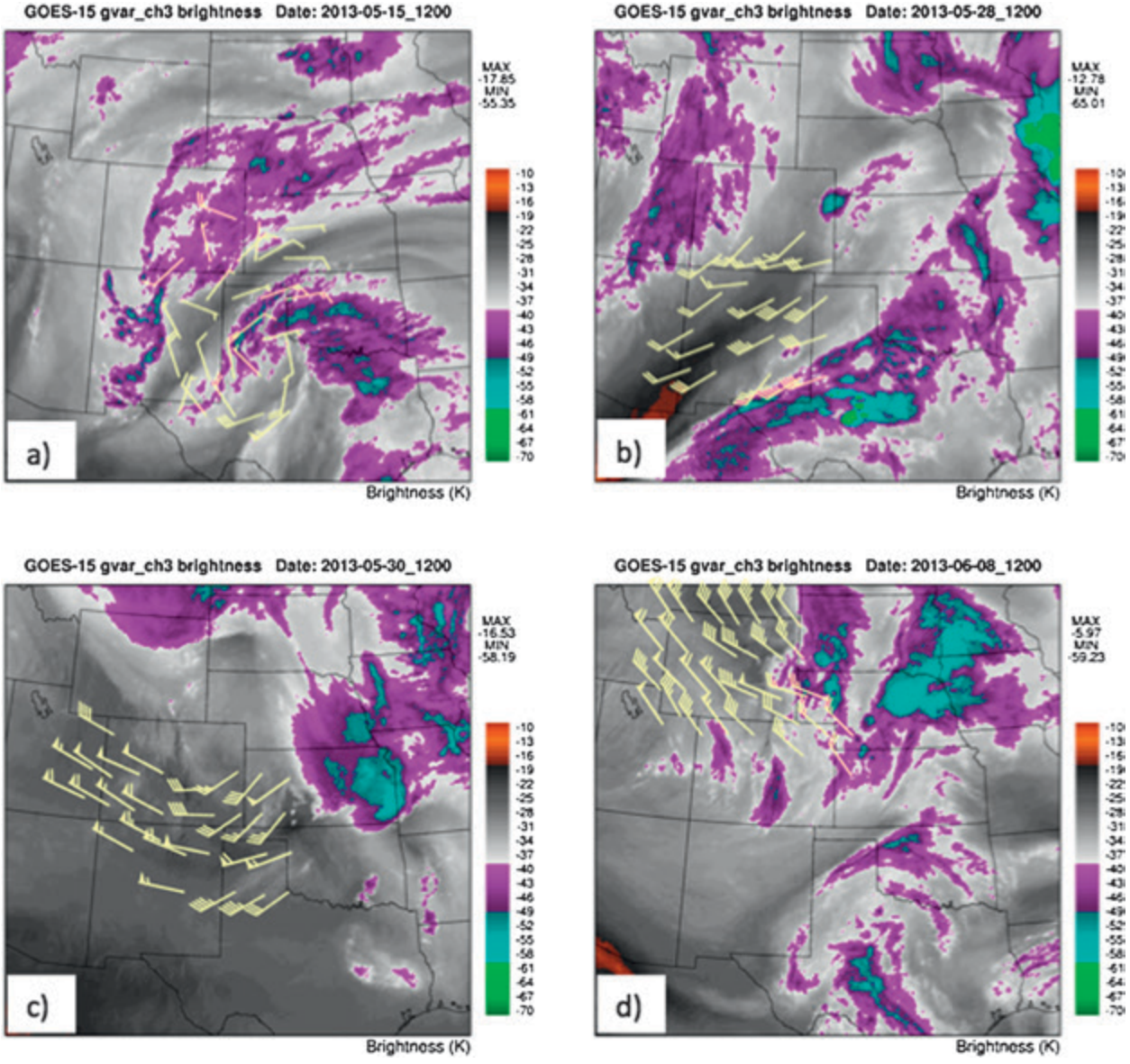

Fig. 7. Examples of morning dropsonde deployments during MPEX, depicting dropsonde winds at 500 hPa obtained during the 5–6-h flight (not time-lag adjusted) on a background water vapor image at 1200 UTC (a) 15 May, (b) 28 May, (c) 30 May, and (d) 8 Jun 2013.

Table 2. Summary of MPEX cases.

IOP No. (date)	Case description	Instruments
1 (15 May)	Upper-level vortex in west Texas. Widespread convection and severe weather in Texas and Oklahoma (unexpected tornadoes near Dallas).	GV drops: 27 Upsondes: 5
2 (16 May)	Upper-tropospheric vortex over Colorado. Convection in Kansas and Nebraska.	GV drops: 30 Upsondes: 6
3 (18 May)	Midtropospheric vortex in the Texas Panhandle. Convection in Oklahoma and Kansas (tornadic supercell in west-central Kansas).	GV drops: 17 Upsondes: 16
4 (19 May)	An upper-level jet–front system over Colorado and New Mexico. Tornado outbreak in eastern Oklahoma and Kansas.	GV drops: 29 Upsondes: 17
5 (20 May)	Strong upper-level trough and jet over New Mexico and Oklahoma. Tornado outbreak targeted in central Oklahoma (Moore, Oklahoma, tornado).	Upsondes: 18
6 (21 May)	An upper-level trough in New Mexico and west Texas. Widespread convection in east-central Texas.	GV drops: 27
7 (23 May)	Surface front in northwestern Texas along with weak, upper-tropospheric potential vorticity (PV) features in New Mexico and Arizona. Severe convection in west-central Texas.	GV drops: 29 Upsondes: 23
8 (27 May)	An upper-tropospheric feature over the intermountain region embedded within subtropical southwesterly flow contributes to locally intense convection in western and south-central Nebraska and north-central Kansas.	GV drops: 29 Upsondes: 22
9 (28 May)	Weak upper-level features in southwesterly flow over New Mexico. Strong convection in southwestern Kansas and the Oklahoma and Texas Panhandles.	GV drops: 21 Upsondes: 18
10 (29 May)	Deep trough over the intermountain region with strong southwesterly flow over the high plains. Widespread convection from Texas through South Dakota. Bow echo in western Oklahoma and Texas Panhandle.	Upsondes: 20
11 (30 May)	Strong trough and associated jet over Wyoming, Colorado, and New Mexico. Widespread severe convection in eastern Kansas, east-central Oklahoma, and extending northeastward into Illinois.	GV drops: 26 Upsondes: 26
12 (31 May)	Strong jet over Colorado, New Mexico, and west Texas. Tornadic storms in central and eastern Oklahoma, extending northeastward into Missouri and Illinois (El Reno, Oklahoma, tornado).	GV drops: 28 Upsondes: 17
13 (3 Jun)	An upper-level trough and associated cold front in Wyoming and Colorado. Scattered convection from western Nebraska southward to the Oklahoma Panhandle.	GV drops: 32 Upsondes: 17
14 (4 Jun)	Dryline targeted in Texas Panhandle in the wake of an earlier MCS. Only weak convection ensued.	Upsondes: 15
15 (8 Jun)	A weak trough embedded within strong northwesterly flow over Wyoming and Colorado. Widespread convection from the Oklahoma Panhandle northeastward into Iowa.	GV drops: 31 Upsondes: 22
16 (11 Jun)	An upper-level trough in northern Utah embedded in southwesterly flow. Convection from Montana southeastward to northern Nebraska.	GV drops: 33 Upsondes: 21
17 (12 Jun)	Upper-level trough extending from North Dakota southward through Nebraska. Severe convection from Iowa eastward (a strong derecho was anticipated from Chicago eastward). A weak, upper-level feature in northern Utah contributes to convection in northeastern Wyoming.	GV drops: 33 Upsondes: 19
18 (14 Jun)	A weak trough and associated surface front embedded in southwesterly flow over Colorado and Wyoming. Moderate convection from southeastern Colorado northeastward to south-central Nebraska.	GV drops: 33 Upsondes: 8

high-impact storms would likely develop on the afternoon of 19 May, with a cluster in central Oklahoma and strong mesoscale convective systems over central and eastern Kansas (Figs. 10, 11). Many of the forecast storms also displayed high values of updraft helicity (e.g., >150 $m^2 s^{-2}$; Kain et al. 2010b), suggesting that the storms would likely be supercellular in nature (Fig. 11a). Given the potential high-impact event, we then sought to determine if suitable uncertainty existed for a targeting mission. Automated algorithms identified preliminary forecast features for ESA guidance that helped identify regions of forecast uncertainty. Still, not all forecast regions were associated with robust ESA patterns, such as the precipitation area forecast over central Oklahoma. As such, a manual box was defined over the region of moderate probabilities of convective precipitation in parts of eastern Kansas on the evening of 19 May (Fig. 11b).

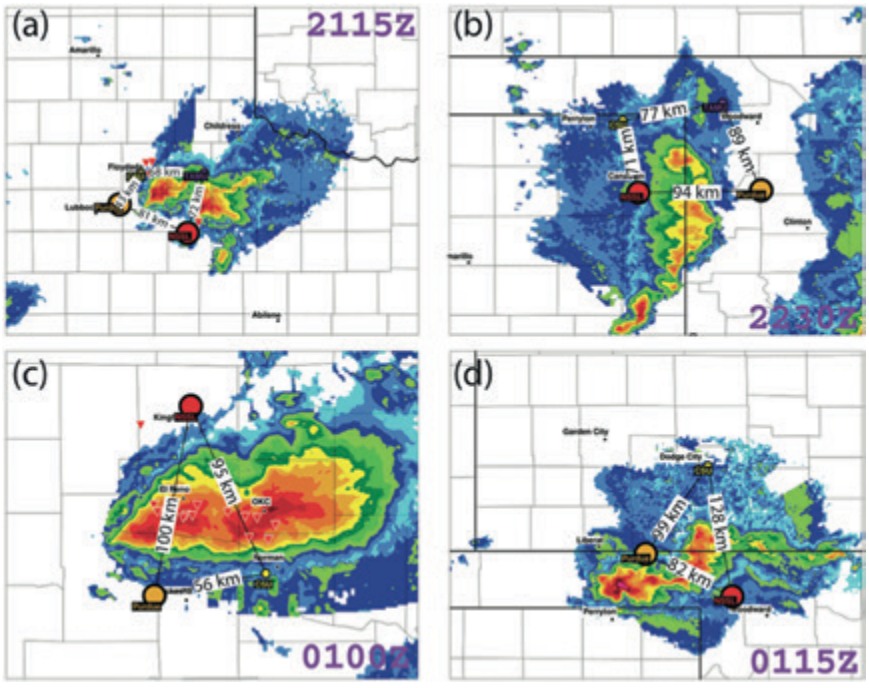

Fig. 8. Examples of upsonde deployments during MPEX on (a) 23 May, (b) 29 May, (c) 31 May, and (d) 3 Jun 2013. Sonde release locations (circles) are overlaid by composite reflectivity factor [NSSL National Mosaic and Multi-Sensor Quantitative Precipitation Estimation (NMQ) product]. Inverted triangles show tornado reports.

Precipitation forecasts over eastern Kansas were characterized by a clear sensitivity to upstream features in the 24-h forecast, which was centered on the dropsonde mission window (Fig. 12). At

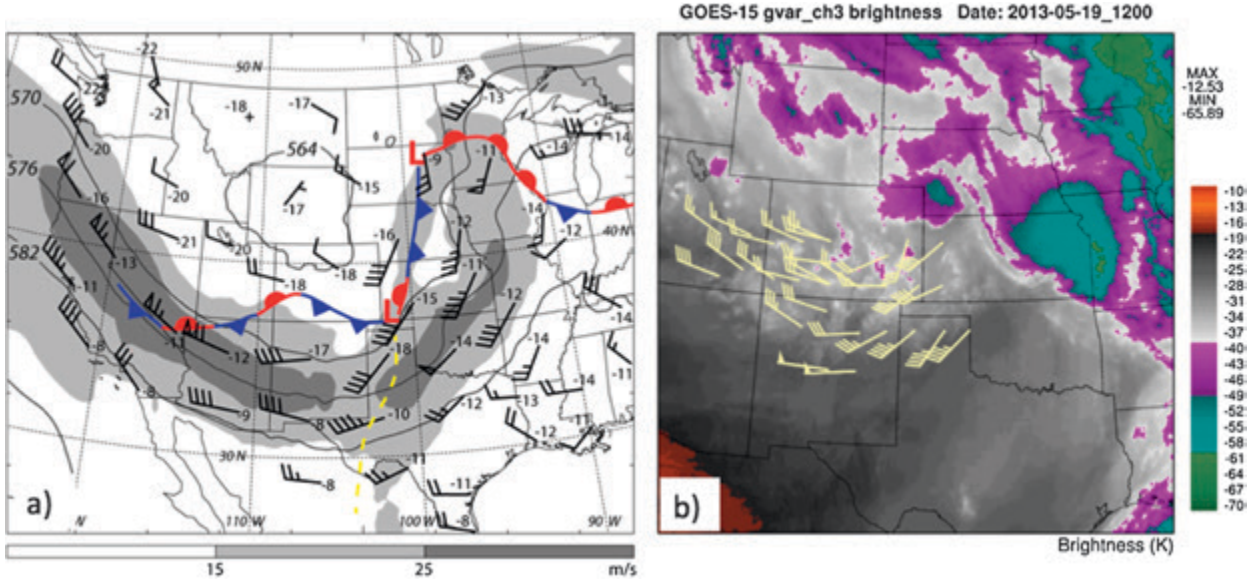

Fig. 9. (a) 500-hPa analysis and significant surface features and (b) satellite water vapor, including dropsonde winds at 500 hPa from the early morning GV mission, at 1200 UTC 19 May 2013. The yellow dashed line in (a) indicates the location of the surface dryline. Other frontal symbols are standard.

this time, the sensitivity magnitude is maximized on the southern edge of the broad western trough over northern New Mexico and Arizona, such that increasing the 500-hPa vorticity, akin to shifting the position of the trough to the south, is associated with increased precipitation in the eastern Kansas box 12 h later. Indeed, this particular region at the base of the trough was also the region that was forecast to propagate eastward over Oklahoma later in the day, contributing to the generation of the local convective environment as well as the triggering of the convection itself. Moreover, the ESA calculation suggested that dropsonde points located along the Colorado–New Mexico border would produce the largest reduction in the variance of the precipitation forecast within the eastern Kansas box (Fig. 12b). Based on available guidance, it was anticipated that dropsonde observations collected from eastern Utah through southwestern Colorado and northern New Mexico would better document this jet and upper-level frontal structure (Fig. 9b) and would have the potential to improve later forecasts.

The updated ensemble forecasts from 1200 UTC 19 May, valid 0000 UTC 20 May (Figs. 13, 14), continued to forecast an outbreak of severe convection from central Oklahoma and northeastward through central and eastern Kansas, Iowa, and eastern Minnesota. The primary convective mode produced in these forecasts was multiple, linear, bow-shaped convective segments from Kansas northward into Iowa, with a more isolated cluster of strong cells in central Oklahoma. The analysis system used for the real-time ensemble forecasts was updated every 6 h, so after four additional rounds of observation information, this day-1 forecast (Figs. 13, 14) was considerably more certain of the forecast evolution of storms relative to the earlier day-2 forecast (Figs. 10, 11). Nevertheless, ESA applied to the morning analysis still indicated sensitive observations within the region earlier targeted for sampling (not shown). The reflectivity frequency plots constructed from the ensemble suggests a fairly consistent forecast for heavy precipitation from Kansas north-northeastward but perhaps a bit less certainty for the cluster of storms being forecast in central Oklahoma. Additionally, the frequency plot for updraft helicity again indicates a high likelihood for supercell storms throughout the region of interest. The observed radar at 0000 UTC (Fig. 13a) clearly shows

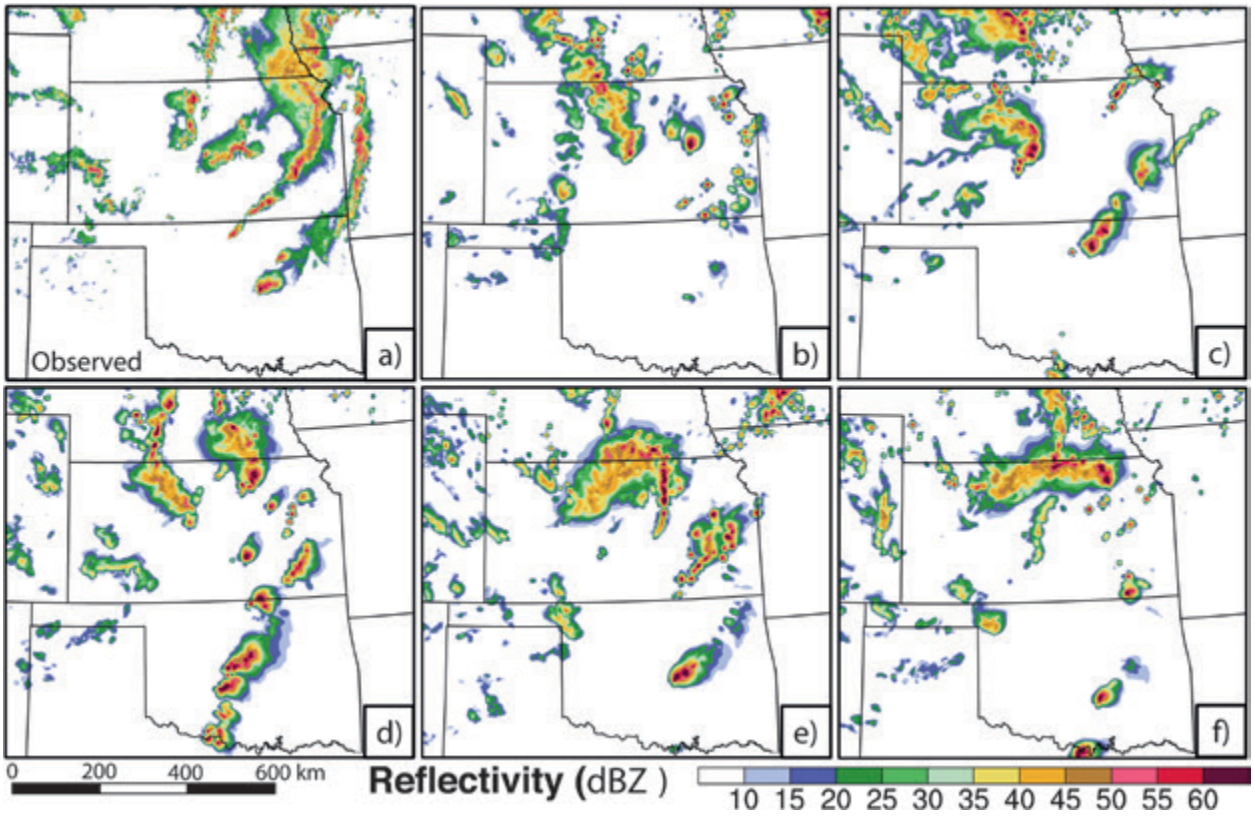

Fig. 10. (a) Composite radar reflectivity (maximum in the column) valid at 0000 UTC 20 May 2013, as compared with (b)–(f) five representative members of the 36-h EnKF forecasts, initialized at 1200 UTC 18 May and valid at 0000 UTC 20 May.

a strong cell in central Oklahoma, which had been significantly tornadic, along with scattered storms across western Missouri. A primary, bow-shaped segment is also present in eastern Kansas, which mostly led to reports of severe winds. Ensemble forecasts largely captured the convective mode and features of the observed event but with notable differences such as the location of the bowing segment in Kansas. Ongoing retrospective studies find the assimilation of dropsonde observations primarily impacts the eastward progression of the bowing segment, improving the timing and location of convection for this event.

Seeking a more isolated convective feature to study, the upsonde teams elected to target a region in north-central Oklahoma for its missions on 19 May. A linear observing array extending from Blackwell, Oklahoma, southward to Perry, Oklahoma, and then Guthrie, Oklahoma, was used to sample the preconvective environment (and one that later supported a tornadic supercell). Each team collected 1900 UTC soundings at their respective locations. Deep convection initiated south and west of this array during the next hour, and a rapidly intensifying cell moving toward the array was chosen for further sampling. Teams redeployed east and south to employ a CDE strategy, with NSSL near Stillwater, Oklahoma; CSU near Perkins, Oklahoma (both north of cell); and the Purdue team south of the cell near Warwick, Oklahoma, and later Rossville, Oklahoma. Several soundings were collected by the teams as the now-tornadic supercell passed through this array. The teams then redeployed south and east to sample other cells that were developing farther southwest. Of note was the tornadic supercell that was sampled at approximately 0045 UTC, within a triangular observing array, with NSSL west of and in the wake of the supercell, CSU north of the supercell, and the Purdue team south of and in the inflow of the supercell (Fig. 15). Ongoing analyses of the soundings (e.g., Fig. 16) and complementary model simulations are showing that the thermodynamic structure of the near-storm atmosphere above the convective boundary layer is relatively unmodified by more isolated deep convection such as supercells. Indeed, for supercells, the most significant upscale feedback identified so far appears to be associated with the storm-generated cold pool. Further analysis of the mobile soundings on this day can be found in Trier et al. (2015).

RESEARCH PLANS AND OPPORTUNITIES. Given the active weather regime and large number of successful deployments, the scientific opportunities afforded by MPEX are plentiful and could contribute significantly to our understanding of the predictability of mesoscale convective weather. To begin, the enhanced temperature, moisture, and wind observations throughout the troposphere will allow us to characterize the upstream and near-convective environments with far more certainty than has generally been available, either operationally or as part of past field campaigns. This will allow for better validation of the existing operational and research analysis systems over the sparsely observed Intermountain West upstream of the central plains' convective events and will also help to identify any systematic and/or significant analysis

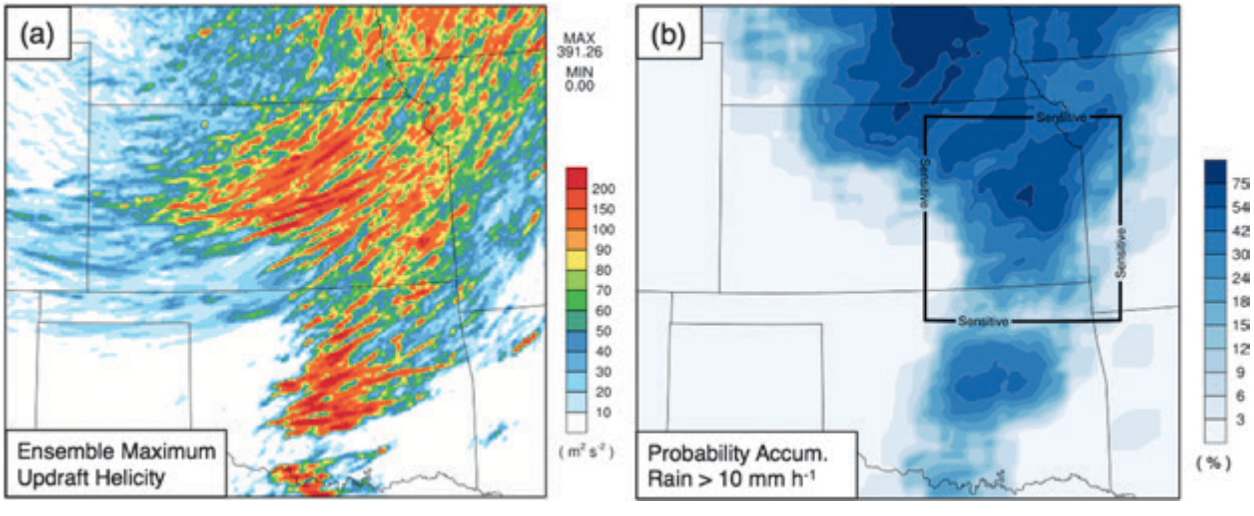

Fig. 11. (a) Cumulative tracks of the ensemble maximum updraft helicity over the period 1800 UTC 19 May–0600 UTC 20 May and (b) ensemble probabilities of accumulated rainfall greater than 10 mm h^{-1} over the period 0000–0300 UTC 20 May, based on EnKF-initialized forecasts from 1200 UTC 18 May 2013. The box labeled "sensitive" in (b) indicates the region used for the ensemble sensitivity analyses, as described in the text.

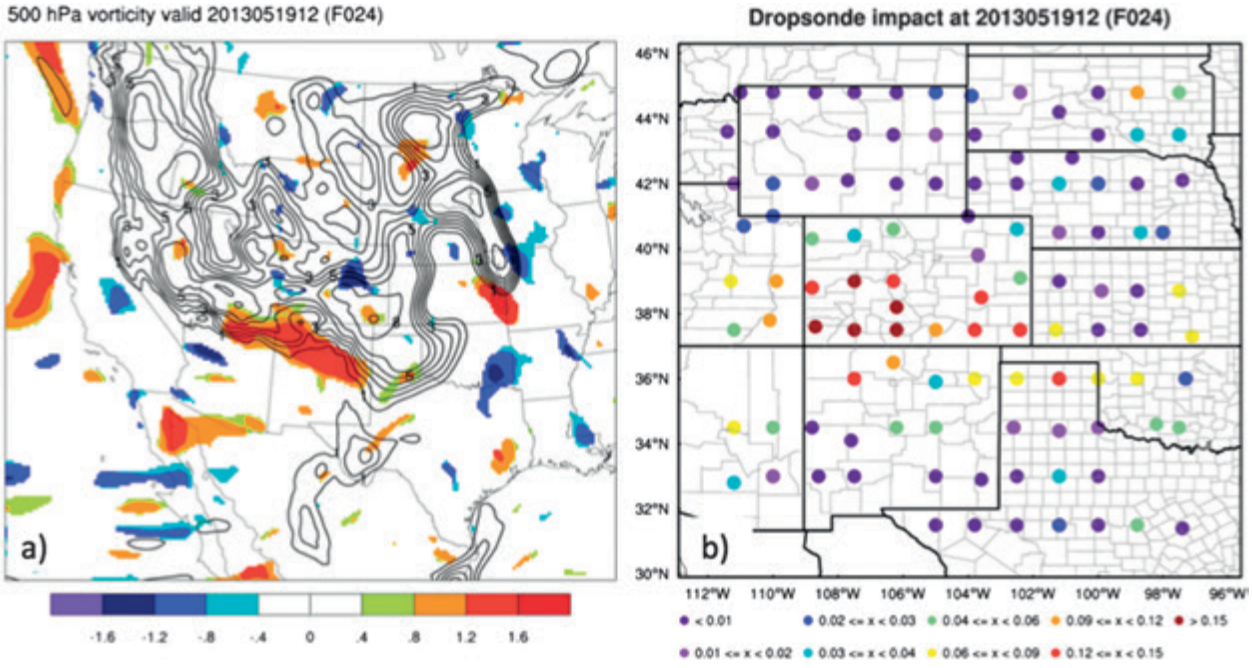

Fig. 12. (a) Sensitivity of the 36–39-h forecast of precipitation averaged over the box in Fig. 11b to the 24-h, 500-hPa vorticity forecast (shading; units are millimeters per standard deviation) for the forecast initialized at 1200 UTC 18 May 2013. The contours denote the ensemble-mean, 500-hPa vorticity (10^{-5} s^{-1}). (b) Hypothetical reduction in the variance of the 36–39-h precipitation averaged over the box in Fig. 11b due to assimilating a dropsonde profile at that point at 1200 UTC 19 May 2013.

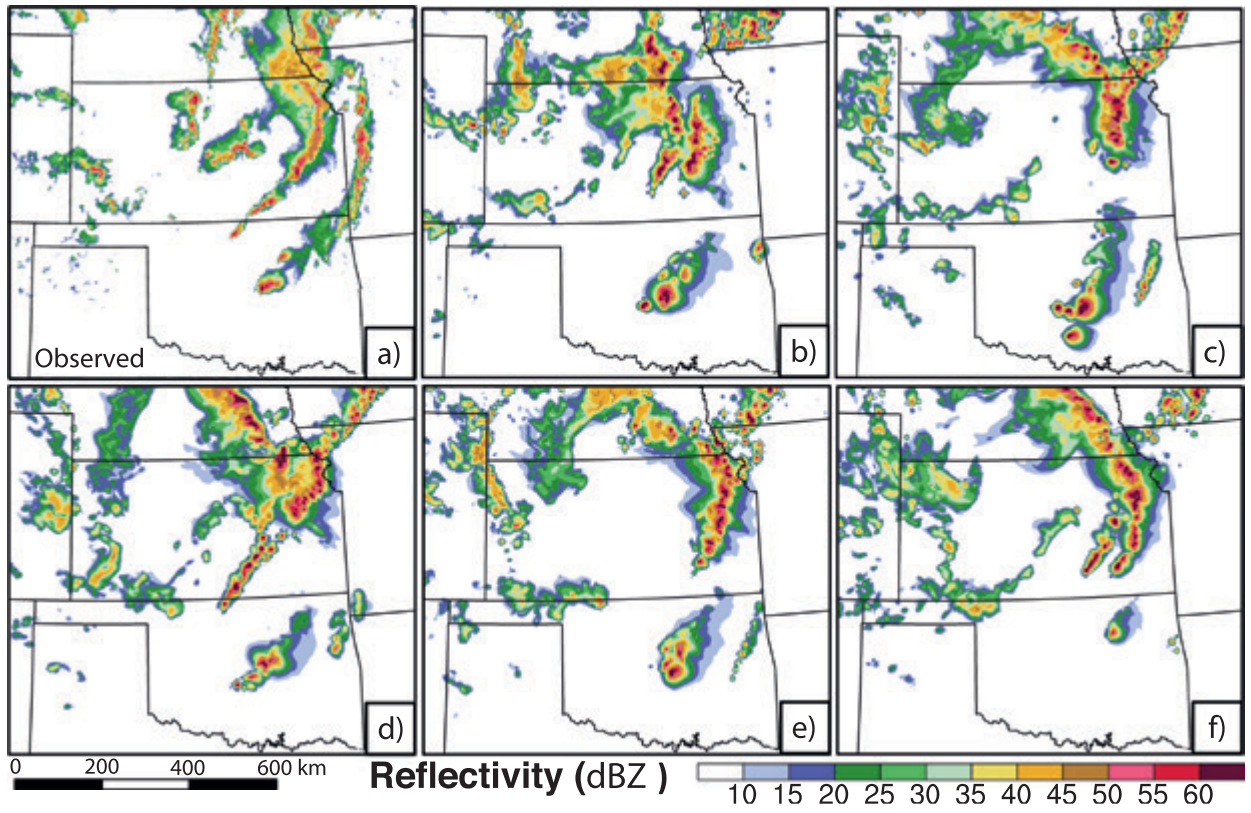

Fig. 13. (a) Composite radar reflectivity (maximum in the column) valid at 0000 UTC 20 May 2013, as compared with (b)–(f) five representative members of the 12-h EnKF forecasts, initialized at 1200 UTC 19 May and valid at 0000 UTC 20 May.

errors during this time period that may have subsequently impacted the convective forecasts. Notably, many strong jet stream–associated upper-level fronts were sampled during the field campaign, offering a unique opportunity to document the mesoscale variations in these features over the complicated terrain of the intermountain regions. More generally, the MPEX observations can be used to better establish the representativeness of the sparse operational radiosonde network over this region.

One of the major questions is whether the relevant analysis errors come from translating midtropospheric features upstream of convection or more local inhomogeneities in moisture, the locations and structure of surface boundaries, and so on. Initial results from the sensitivity analyses suggest that both upstream and local errors are important.

One of the primary goals of MPEX is to use retrospective case studies to assess the impacts of the targeted observations on the subsequent model forecasts. For retrospective events, the assimilation frequency is being increased to hourly cycles to better accommodate the long window of time for GV dropsonde missions to collect observations.

Preliminary results suggest a range of responses to the dropsondes from case to case but generally confirm that the enhanced data can have a positive impact on the subsequent forecasts.

The retrospective experiments with and without dropsonde data also provide an opportunity to assess whether ESA can identify the critical regions where dropsonde data could benefit the forecast. This will be accomplished by repeating the dropsonde experiments described above, but only the subset of dropsondes that overlap with the locations identified by sensitivity analysis [using the algorithm outlined in Torn (2014)] are assimilated. The forecasts generated from these analyses will be compared with the control and an experiment that contains all of the dropsonde data. If the location(s) identified by sensitivity analysis represent the critical initial-condition error, then the impact from assimilating a subset of dropsondes should be similar to assimilating all dropsondes.

Forecast sensitivity analysis also affords the opportunity to better understand the processes that impact the predictability of convection events. As an example, sensitivity analysis identified that forecast metrics that measure convection on 19 May (i.e., area-averaged precipitation or vertical kinetic energy) were sensitive to the southern extent of the upper trough over Colorado and to the lower-tropospheric meridional moisture transport over north-central Texas at 1200 UTC (Torn and Romine 2015). Future work will evaluate the relative importance of each of these sensitivities, apply processed-based studies to understand why sensitivity analysis identifies these features, and compare the results to other strongly forced events during MPEX, such as on 30 May. Ultimately, these studies could help us identify which weather regimes could benefit the most from additional data, as might be afforded by targeted dropsonde or upsonde operations.

The afternoon upsondes will be especially useful for producing composite inflow soundings for the many severe storms that were sampled and will also

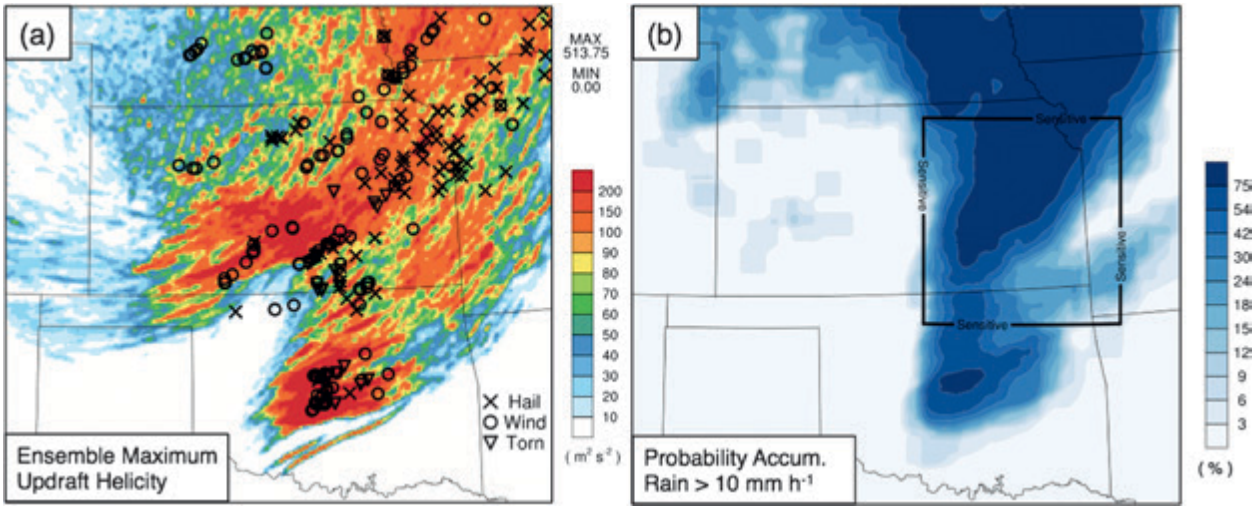

Fig. 14. As in Fig. 11, but based on EnKF-initialized forecasts from 1200 UTC 19 May 2013 and overlain in (a) are preliminary storm reports as compiled by NOAA/SPC during the same period as the forecast.

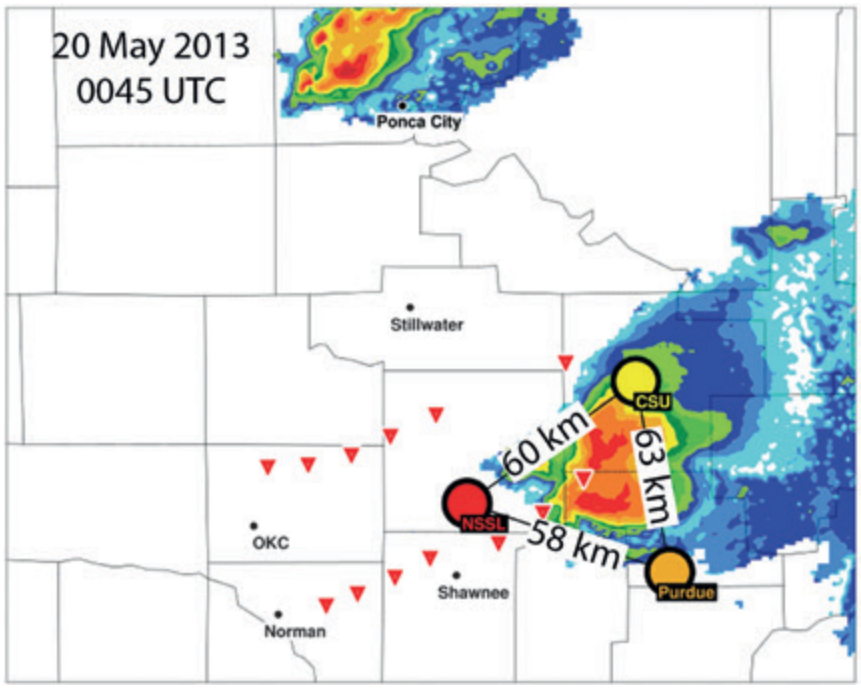

Fig. 15. As in Fig. 8, but for the upsonde deployment on 19 May 2013.

be used to produce composites of triangle calculations over different stages of storm evolution, which will help assess the impacts of the convection on the regional environment. More generally, the upsonde data will be used to verify the earlier model forecasts, especially offering valuable insights into the processes of convective initiation as represented by the high-resolution forecasts. Furthermore, the upsonde and available radar reflectivity and velocity data will be assimilated to create enhanced storm-scale analyses for input to subsequent convective-scale forecasts.

Given the extensive set of mesoscale observations obtained during MPEX, the ultimate goal of the related research is to better establish how mesoscale analysis errors impact subsequent convective-scale forecasts over a 0–24-h time scale and perhaps beyond. An important component of this is to clarify where the weaknesses reside in our current observational system and, in particular, which variables generate the largest sensitivities in the subsequent convective forecasts. However, not only will MPEX afford researchers the opportunity to help identify any systematic and/or specifically significant analysis errors, but it will also help expedite the identification of systematic errors or shortcomings in the cycled data analysis system and/or numerical model system and their components (e.g., subgrid parameterizations).

Finally, MPEX will also serve as an opportunity to evaluate the practical and intrinsic short-range predictability of more specific attributes of convection. For instance, research is ongoing to quantify the practical predictability of convective initiation, how it is influenced by the assimilation of MPEX dropsonde observations, to examine how both observational and PBL parameterization uncertainty limits its intrinsic predictability, and to identify systematic model biases influencing the skillful prediction of convective initiation.

ACKNOWLEDGMENTS. We would like to gratefully acknowledge support from the National Science Foundation (NSF) and the National Oceanic and Atmospheric Administration (NOAA). The field project support provided by NCAR/EOL staff, especially Jim Moore, Steve Williams, Brigitte Baeuerle, and Greg Stossmeister, and the computer resources and technical support offered by NCAR/CISL and Wei Wang, Kate Fossell, and Dave Ahijevych of NCAR/MMM are also gratefully appreciated. Thanks also go to Don Conlee of Texas A&M University and to the many student participants involved in the day-to-day operations of the field campaign, especially in support of the mobile upsonde operations, including Matt Paulus, Vanessa Vincente, John Peters, and Adam Rydbeck from Colorado State University; Logan Dawson and Joe Woznicki from Purdue University; Chris Kerr, Stuart Miller, Derek Stratman, Mike Vandenberg, Stacey Hitchcock, Larissa Reames, and Sean Waugh from the University of Oklahoma; and Corey Guastini from the University at Albany. Data from the field campaign can be found at the NCAR/EOL field projects catalog (www.eol.ucar.edu/projects/mpex/). NCAR is operated by UCAR under sponsorship of the NSF.

APPENDIX: MOBILE UPSONDE SYSTEMS.

The Purdue and NSSL systems are composed of the iMet-3050 and iMet-3150 403-MHz GPS radiosonde receiver and antenna (manufactured by International Met Systems). Laptop computers running the iMETOS were used to process the radiosonde data, which were collected using iMet-1-AB 403-MHz GPS radio-

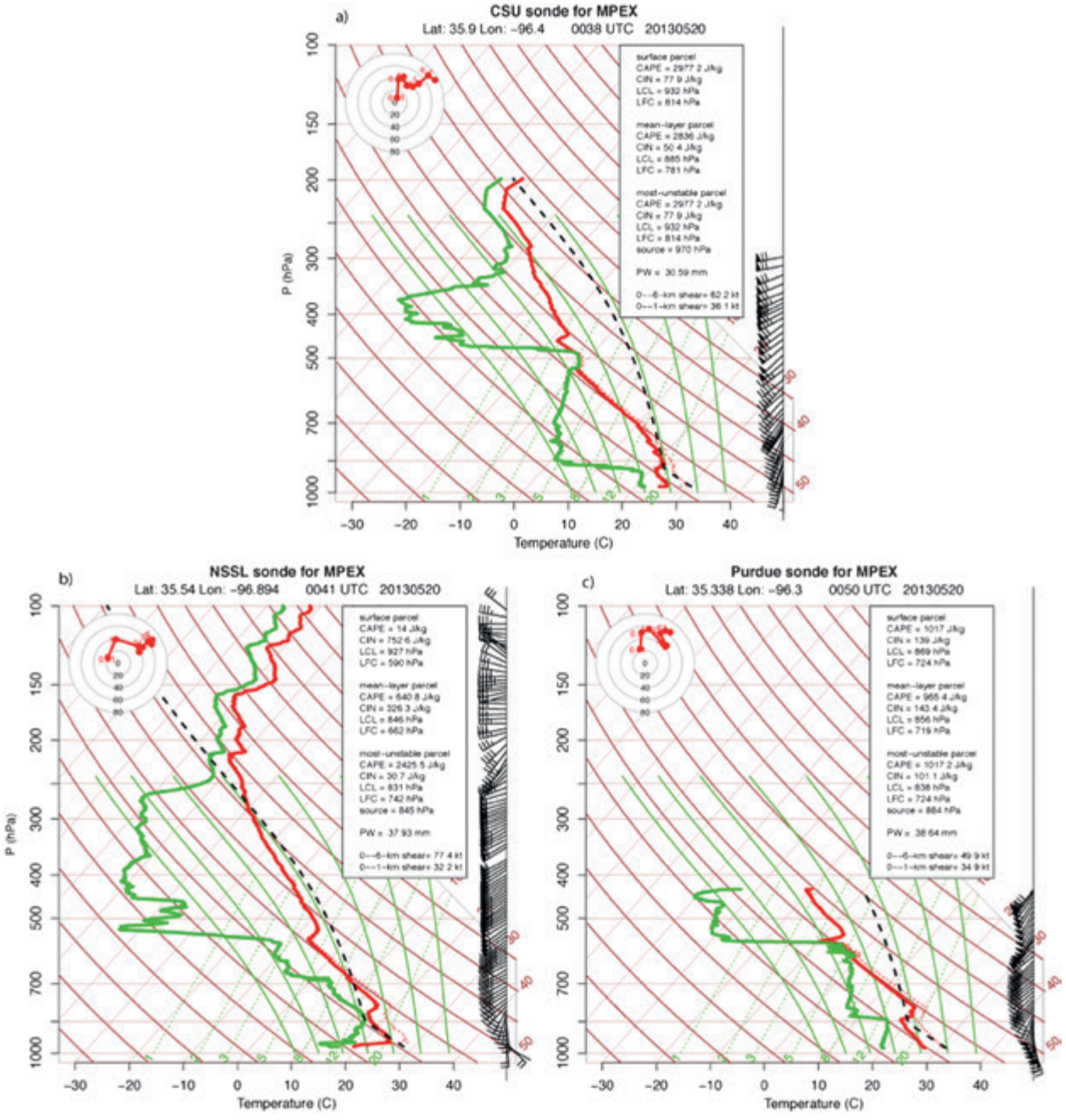

Fig. 16. Sample soundings from the upsonde deployment portrayed in Fig. 15 from the (a) CSU, (b) NSSL, and (c) Purdue mobile sounding units. Dashed black lines indicate the parcel path for a 500-m, mean-layer, lifted parcel. Calculations of thermodynamic quantities should be viewed with caution because not all soundings reached the level of neutral buoyancy.

sondes with a pressure sensor; preflight calibration is not needed with the iMet-1-ABs. The sondes were suspended from 200-g latex balloons, with a dereeler and 30-m string.

The CSU system is a Digicora MW21 using Vaisala RS92 sondes with a GC25 (ground check system). It uses a GPS antenna for wind finding and a UHF antenna operating around 400 Hz for transmitting the signal from the sonde to the ground system. Similarly, a laptop computer running the Digicora software was used to process the radiosonde data. As with the NSSL and Purdue systems, the sondes were suspended from 200-g latex balloons, with a dereeler and 30-m string.

REFERENCES

Aberson, S. D., 2003: Targeted observations to improve operational tropical cyclone track forecast guidance. *Mon. Wea. Rev.*, **131**, 1613–1628, doi:10.1175//2550.1.

Anabor, V., D. J. Stensrud, and O. L. L. de Moraes, 2009: Simulation of a serial upstream-propagating mesoscale convective system event over southeastern South America. *Mon. Wea. Rev.*, **137**, 2144–2163, doi:10.1175/2008MWR2617.1.

Ancell, B., and G. J. Hakim, 2007: Comparing adjoint- and ensemble-sensitivity analysis with applications to observation targeting. *Mon. Wea. Rev.*, **135**, 4117–4134, doi:10.1175/2007MWR1904.1.

Anderson, J. L., T. Hoar, K. Raeder, H. Liu, N. Collins, R. Torn, and A. Avellano, 2009: The Data Assimilation Research Testbed: A community facility. *Bull. Amer. Meteor. Soc.*, **90**, 1283–1296, doi:10.1175/2009BAMS2618.1.

Barth, M. C., and Coauthors, 2015: The Deep Convective Clouds and Chemistry (DC3) field campaign. *Bull. Amer. Meteor. Soc.*, **96**, 1281–1309, doi:10.1175/BAMS-D-13-00290.1.

Benjamin, S. G., B. D. Jamison, W. R. Moninger, S. R. Sahm, B. E. Schwartz, and T. W. Schlatter, 2010: Relative short-range forecast impact from aircraft, profiler, radiosonde, VAD, GPS-PW, METAR, and mesonet observations via the RUC hourly assimilation cycle. *Mon. Wea. Rev.*, **138**, 1319–1343, doi:10.1175/2009MWR3097.1.

Brooks, H. E., C. A. Doswell III, and J. Cooper, 1994: On the environments of tornadic and nontornadic mesocyclones. *Wea. Forecasting*, **9**, 606–618, doi:10.1175/1520-0434(1994)009<0606:OTEOTA>2.0.CO;2.

Clark, A. J., W. A. Gallus Jr., M. Xue, and F. Kong, 2010a: Growth of spread in convection-allowing and convection-parameterizing ensembles. *Wea. Forecasting*, **25**, 594–612, doi:10.1175/2009WAF2222318.1.

——, ——, ——, and ——, 2010b: Convection-allowing and convection-parameterizing ensemble forecasts of a mesoscale convective vortex and associated severe weather environment. *Wea. Forecasting*, **25**, 1052–1081, doi:10.1175/2010WAF2222390.1.

——, and Coauthors, 2012: An overview of the 2010 Hazardous Weather Testbed experimental forecast spring experiment. *Bull. Amer. Meteor. Soc.*, **93**, 55–74, doi:10.1175/BAMS-D-11-00040.1.

Coniglio, M. C., K. L. Elmore, J. S. Kain, S. J. Weiss, M. Xue, and M. L. Weisman, 2010: Evaluation of WRF model output for severe weather forecasting from the 2008 NOAA Hazardous Weather Testbed spring experiment. *Wea. Forecasting*, **25**, 408–427, doi:10.1175/2009WAF2222258.1.

——, J. Correia Jr., P. T. Marsh, and F. Kong, 2013: Verification of convection-allowing WRF model forecasts of the planetary boundary layer using sounding observations. *Wea. Forecasting*, **28**, 842–862, doi:10.1175/WAF-D-12-00103.1.

Dabberdt, W. F., and Coauthors, 2000: Forecast issues in the urban zone: Report of the 10th Prospectus Development Team of the U.S. Weather Research Program. *Bull. Amer. Meteor. Soc.*, **81**, 2047–2064, doi:10.1175/1520-0477(2000)081<2047:FIITUZ>2.3.CO;2.

Davis, C., and Coauthors, 2004: The Bow Echo and MCV Experiment: Observations and opportunities. *Bull. Amer. Meteor. Soc.*, **85**, 1075–1093, doi:10.1175/BAMS-85-8-1075.

Done, J., C. A. Davis, and M. Weisman, 2004: The next generation of NWP: Explicit forecasts of convection using the Weather Research and Forecasting (WRF) model. *Atmos. Sci. Lett.*, **5**, 110–117, doi:10.1002/asl.72.

Droegemeier, K. K., 1990: Toward a science of storm scale prediction. Preprints, *16th Conf. on Severe Local Storms*, Kananaskis Park, AB, Canada, Amer. Meteor. Soc., 256–262.

——, 1997: The numerical prediction of thunderstorms: Challenges, potential benefits and results from real-time operational tests. *WMO Bull.*, **46**, 324–336.

——, and Coauthors, 1996: Realtime numerical prediction of storm-scale weather during VORTEX '95: Goals and methodology. Preprints, *18th Conf. on Severe Local Storms*, San Francisco, CA, Amer. Meteor. Soc., 6–10.

——, and Coauthors, 2000: Hydrological aspects of weather prediction and flood warnings: Report of the Ninth Prospectus Development Team of the U.S. Weather Research Program. *Bull. Amer. Meteor. Soc.*, **81**, 2665–2680, doi:10.1175/1520-0477(2000)081<2665:HAOWPA>2.3.CO;2.

Duda, J. D., and W. A. Gallus, Jr., 2013: The impact of large-scale forcing on skill of simulated convective initiation and upscale evolution with convection-allowing grid spacings in the WRF. *Wea. Forecasting*, **28**, 994–1018, doi:10.1175/WAF-D-13-00005.1.

Fritsch, J. M., and R. A. Maddox, 1981: Convectively driven mesoscale pressure systems aloft. Part I: Observations. *J. Appl. Meteor.*, **20**, 9–19, doi:10.1175/1520-0450(1981)020<0009:CDMWSA>2.0.CO;2.

——, and Coauthors, 1998: Quantitative precipitation forecasting: Report of the Eighth Prospectus Development Team, U.S. Weather Research Program. *Bull. Amer. Meteor. Soc.*, **79**, 285–299, doi:10.1175/1520-0477(1998)079<0285:QPFROT>2.0.CO;2.

Gamache, J. F., and R. A. Houze Jr., 1982: Mesoscale air motions associated with a tropical squall line.

Mon. Wea. Rev., **110**, 118–135, doi:10.1175/1520-0493(1982)110<0118:MAMAWA>2.0.CO;2.

Haggerty, J., K. Schick, M. J. Mahoney, and B. Lim, 2014: The NCAR microwave temperature profiler: Data applications from recent field deployments. *Proc. 13th Specialists Meeting on Microwave Radiometry and Remote Sensing of the Environment*, Pasadena, CA, IEEE, 133–135, doi:10.1109/MicroRad.2014.6878924.

Hock, T. F., and J. L. Franklin, 1999: The NCAR GPS dropwindsonde. *Bull. Amer. Meteor. Soc.*, **80**, 407–420, doi:10.1175/1520-0477(1999)080<0407:TNGD>2.0.CO;2.

Hohenegger, C., and C. Schär, 2007: Atmospheric predictability at synoptic versus cloud-resolving scales. *Bull. Amer. Meteor. Soc.*, **88**, 1783–1793, doi:10.1175/BAMS-88-11-1783.

Houze, R. A., Jr., 1977: Structure and dynamics of a tropical squall line system. *Mon. Wea. Rev.*, **105**, 1540–1567, doi:10.1175/1520-0493(1977)105<1540:SADOAT>2.0.CO;2.

——, and A. K. Betts, 1981: Convection in GATE. *Rev. Geophys. Space Phys.*, **19**, 541–576, doi:10.1029/RG019i004p00541.

Ikeda, K., M. Steiner, J. Pinto, and C. Alexander, 2013: Evaluation of cold season precipitation forecasts generated by the hourly updating high-resolution rapid refresh model. *Wea. Forecasting*, **28**, 921–939, doi:10.1175/WAF-D-12-00085.1.

Joly, A., and Coauthors, 1999: Overview of the field phase of the Fronts and Atlantic Storm-Track Experiment (FASTEX) project. *Quart. J. Roy. Meteor. Soc.*, **125**, 3131–3163, doi:10.1002/qj.49712556103.

Kain, J. S., S. J. Weiss, M. E. Baldwin, G. W. Carbin, D. A. Bright, J. J. Levit, and J. A. Hart, 2005: Evaluating high-resolution configurations of the WRF model that are used to forecast severe convective weather: The 2005 SPC/NSSL spring program. Preprints, *21st Conf. on Weather Analysis and Forecasting/17th Conf. on Numerical Weather Prediction*, Washington, D.C., Amer. Meteor. Soc., 2A.5. [Available online at https://ams.confex.com/ams/pdfpapers/94843.pdf.]

——, ——, J. J. Levit, M. E. Baldwin, and D. R. Bright, 2006: Examination of convective allowing configurations of the WRF model for the prediction of severe convective weather: The SPC/NSSL spring program 2004. *Wea. Forecasting*, **21**, 167–181, doi:10.1175/WAF906.1.

——, and Coauthors, 2008: Some practical considerations for the first generation of operational convection allowing NWP: How much resolution is enough? *Wea. Forecasting*, **23**, 931–952, doi:10.1175/WAF2007106.1.

——, and Coauthors, 2010a: Assessing advances in the assimilation of radar data and other mesoscale observations within a collaborative forecasting–research environment. *Wea. Forecasting*, **25**, 1510–1521, doi:10.1175/2010WAF2222405.1.

——, S. R. Dembek, S. J. Weiss, J. L. Case, J. J. Levit, and R. A. Sobash, 2010b: Extracting unique information from high-resolution forecast models: Monitoring selected fields and phenomena every time step. *Wea. Forecasting*, **25**, 1536–1542, doi:10.1175/2010WAF2222430.1.

——, and Coauthors, 2013: A feasibility study for probabilistic convection initiation forecasts based on explicit numerical guidance. *Bull. Amer. Meteor. Soc.*, **94**, 1213–1225, doi:10.1175/BAMS-D-11-00264.1.

Keyser, D. A., and D. R. Johnson, 1984: Effects of diabatic heating on the ageostrophic circulation of an upper tropospheric jet streak. *Mon. Wea. Rev.*, **112**, 1709–1724, doi:10.1175/1520-0493(1984)112<1709:EODHOT>2.0.CO;2.

Lean, H. W., P. A. Clark, M. Dixon, N. M. Roberts, A. Fitch, R. Forbes, and C. Halliwell, 2008: Characteristics of high-resolution versions of the Met Office Unified Model for forecasting convection over the United Kingdom. *Mon. Wea. Rev.*, **136**, 3408–3424, doi:10.1175/2008MWR2332.1.

Leary, C. A., 1979: Behavior of the wind field in the vicinity of a cloud cluster in the intertropical convergence zone. *J. Atmos. Sci.*, **36**, 631–639, doi:10.1175/1520-0469(1979)036<0631:BOTWFI>2.0.CO;2.

Lilly, D. K., 1990: Numerical prediction of thunderstorms—Has its time come? *Quart. J. Roy. Meteor. Soc.*, **116**, 779–798, doi:10.1002/qj.49711649402.

Maddox, R. A., 1980: Mesoscale convective complexes. *Bull. Amer. Meteor. Soc.*, **61**, 1374–1387, doi:10.1175/1520-0477(1980)061<1374:MCC>2.0.CO;2.

Menard, R. D., and J. M. Fritsch, 1989: A mesoscale convective complex-generated inertially stable warm core vortex. *Mon. Wea. Rev.*, **117**, 1237–1261, doi:10.1175/1520-0493(1989)117<1237:AMCCGI>2.0.CO;2.

Metz, N. D., and L. F. Bosart, 2010: Derecho and MCS development, evolution, and multiscale interactions during 3–5 July 2003. *Mon. Wea. Rev.*, **138**, 3048–3070, doi:10.1175/2010MWR3218.1.

Ninomiya, K., 1971a: Dynamical analysis of outflow from tornado-producing thunderstorms as revealed by ATS III pictures. *J. Appl. Meteor.*, **10**, 275–294, doi:10.1175/1520-0450(1971)010<0275:DAOOFT>2.0.CO;2.

——, 1971b: Mesoscale modification of synoptic situations from thunderstorm development

as revealed by ATS III and aerological data. *J. Appl. Meteor.*, **10**, 1103–1121, doi:10.1175/1520-0450(1971)010<1103:MMOSSF>2.0.CO;2.

Parker, M. D., 2014: Composite VORTEX2 supercell environments from near-storm soundings. *Mon. Wea. Rev.*, **142**, 508–529, doi:10.1175/MWR-D-13-00167.1.

Perkey, D. J., and R. A. Maddox, 1985: A numerical investigation of a mesoscale convective system. *Mon. Wea. Rev.*, **113**, 553–566, doi:10.1175/1520-0493(1985)113<0553:ANIOAM>2.0.CO;2.

Riehl, H., 1959: On the production of kinetic energy from condensation heating. *The Atmosphere and the Sea in Motion: Scientific Contributions to the Rossby Memorial Volume*, B. Bolin, Ed., Rockefeller Institute Press, 509 pp.

Rotach, M. W., and Coauthors, 2009: MAP D-PHASE: Real-time demonstration of weather forecast quality in the alpine region. *Bull. Amer. Meteor. Soc.*, **90**, 1321–1336, doi:10.1175/2009BAMS2776.1.

Schenkman, A. D., M. Xue, A. Shapiro, K. Brewster, and J. Gao, 2011: Impact of CASA radar and Oklahoma Mesonet data assimilation on the analysis and prediction of tornadic mesovortices in an MCS. *Mon. Wea. Rev.*, **139**, 3422–3445, doi:10.1175/MWR-D-10-05051.1.

Schwartz, C. S., and Coauthors, 2009: Next-day convection-allowing WRF model guidance: A second look at 2-km versus 4-km grid spacing. *Mon. Wea. Rev.*, **137**, 3351–3372, doi:10.1175/2009MWR2924.1.

Seity, Y., P. Brousseau, S. Malardel, G. Hello, P. Benard, F. Bouttier, C. Lac, and V. Masson, 2011: The AROME-France convective-scale operational model. *Mon. Wea. Rev.*, **139**, 976–991, doi:10.1175/2010MWR3425.1.

Skamarock, W. C., and Coauthors, 2008: A description of the Advanced Research WRF version 3. NCAR Tech. Note NCAR/TN-475+STR, 113 pp. [Available online at http://www2.mmm.ucar.edu/wrf/users/docs/arw_v3.pdf.]

Smull, B. F., and J. A. Augustine, 1993: Multiscale analysis of a mature mesoscale convective complex. *Mon. Wea. Rev.*, **121**, 103–132, doi:10.1175/1520-0493(1993)121<0103:MAOAMM>2.0.CO;2.

Snively, D. V., and W. A. Gallus Jr., 2014: Prediction of convective morphology in near-cloud-permitting WRF model simulations. *Wea. Forecasting*, **29**, 130–149, doi:10.1175/WAF-D-13-00047.1.

Stensrud, D. J., 1996: Effects of a persistent, midlatitude mesoscale region of convection on the large-scale environment during the warm season. *J. Atmos. Sci.*, **53**, 3503–3527, doi:10.1175/1520-0469(1996)053<3503:EOPMMR>2.0.CO;2.

——, and J. L. Anderson, 2001: Is midlatitude convection an active or a passive player in producing global circulation patterns. *J. Climate*, **14**, 2222–2237, doi:10.1175/1520-0442(2001)014<2222:IMCAAO>2.0.CO;2.

——, and J. Gao, 2010: Importance of horizontally inhomogeneous environmental initial conditions to ensemble storm-scale radar data assimilation and very short-range forecasts. *Mon. Wea. Rev.*, **138**, 1250–1272, doi:10.1175/2009MWR3027.1.

Stratman, D. R., M. C. Coniglio, S. E. Koch, and M. Xue, 2013: Use of multiple verification methods to evaluate forecasts of convection from hot- and cold-start convection-allowing models. *Wea. Forecasting*, **28**, 119–138, doi:10.1175/WAF-D-12-00022.1.

Sun, J., and Y. Zhang, 2008: Analysis and prediction of a squall line observed during IHOP using multiple WSR-88D observations. *Mon. Wea. Rev.*, **136**, 2364–2388, doi:10.1175/2007MWR2205.1.

——, S. B. Trier, Q. Xiao, M. L. Weisman, H. Wang, Z. Ying, M. Xu, and Y. Zhang, 2012: Sensitivity of 0–12-h warm-season precipitation forecasts over the central United States to model initialization. *Wea. Forecasting*, **27**, 832–855, doi:10.1175/WAF-D-11-00075.1.

Szunyogh, I., Z. Toth, R. E. Morss, S. J. Majumdar, B. J. Etherton, and C. H. Bishop, 2000: The effect of targeted dropsonde observations during the 1999 winter storm reconnaissance program. *Mon. Wea. Rev.*, **128**, 3520–3537, doi:10.1175/1520-0493(2000)128<3520:TEOTDO>2.0.CO;2.

Torn, R. D., 2014: The impact of targeted dropwindsonde observations on tropical cyclone intensity forecasts of four weak systems during PREDICT. *Mon. Wea. Rev.*, **142**, 2860–2878, doi:10.1175/MWR-D-13-00284.1.

——, and G. J. Hakim, 2008: Ensemble-based sensitivity analysis. *Mon. Wea. Rev.*, **136**, 663–677, doi:10.1175/2007MWR2132.1.

——, and G. S. Romine, 2015: Sensitivity of central Oklahoma convection forecasts to upstream potential vorticity anomalies during two strongly forced cases during MPEX. *Mon. Wea. Rev.*, **143**, 4064-4087, doi:10.1175/MWR-D-15-0085.1.

Trier, S. B., and R. D. Sharman, 2009: Convection-permitting simulations of the environment supporting widespread turbulence within the upper-level outflow of a mesoscale convective system. *Mon. Wea. Rev.*, **137**, 1972–1990, doi:10.1175/2008MWR2770.1.

——, G. S. Romine, D. A. Ahijevych, R. J. Trapp, R. S. Schumacher, M. C. Coniglio, and D. J. Stensrud, 2015: Mesoscale thermodynamic influences on convection initiation near a surface dryline in a convection-permitting ensemble. *Mon. Wea. Rev.*, **143**, 3726-3753, doi:10.1175/MWR-D-15-0133.1.

Vandenberg, M. A., M. C. Coniglio, and A. J. Clark, 2014: Comparison of next-day convection-allowing forecasts of storm motion on 1- and 4-km grids. *Wea. Forecasting*, **29**, 878–893, doi:10.1175/WAF-D-14-00011.1.

Wandishin, M. S., D. J. Stensrud, S. L. Mullen, and L. J. Wicker, 2010: On the predictability of mesoscale convective systems: Three-dimensional simulations. *Mon. Wea. Rev.*, **138**, 863–885, doi:10.1175/2009MWR2961.1.

Weisman, M. L., C. A. Davis, W. Wang, K. W. Manning, and J. B. Klemp, 2008: Experiences with 0–36-h explicit convective forecasts with the WRF-ARW model. *Wea. Forecasting*, **23**, 407–437, doi:10.1175/2007WAF2007005.1.

Weiss, S. J., J. S. Kain, J. J. Levit, M. E. Baldwin, and D. R. Bright, 2004: Examination of several different versions of the WRF model for the prediction of severe convective weather: The SPC/NSSL Spring Program 2004. Preprints, *22nd Conf. on Severe Local Storms*, Hyannis, MA, Amer. Meteor. Soc., 17.1. [Available online at https://ams.confex.com/ams/11aram22sls/techprogram/paper_82052.htm.]

——, and Coauthors, 2007: The NOAA Hazardous Weather Testbed: Collaborative testing of ensemble and convection-allowing WRF models and subsequent transfer to operations at the Storm Prediction Center. Preprints, *22nd Conf. on Weather Analysis and Forecasting/18th Conf. on Numerical Weather Prediction*, Park City, UT, Amer. Meteor. Soc., 6B.4. [Available online at https://ams.confex.com/ams/pdfpapers/124772.pdf.]

Wetzel, P. J., W. R. Cotton, and R. L. McAnelly, 1983: A long-lived mesoscale convective complex. Part II: Evolution and structure of the mature complex. *Mon. Wea. Rev.*, **111**, 1919–1937, doi:10.1175/1520-0493(1983)111<1919:ALLMCC>2.0.CO;2.

Wolf, B. J., and D. R. Johnson, 1995a: The mesoscale forcing of a midlatitude upper-tropospheric jet streak by a simulated convective system. Part I: Mass circulation and ageostrophic processes. *Mon. Wea. Rev.*, **123**, 1059–1087, doi:10.1175/1520-0493(1995)123<1059:TMFOAM>2.0.CO;2.

——, and ——, 1995b: The mesoscale forcing of a midlatitude upper-tropospheric jet streak by a simulated convective system. Part II: Kinetic energy and resolution analysis. *Mon. Wea. Rev.*, **123**, 1088–1111, doi:10.1175/1520-0493(1995)123<1088:TMFOAM>2.0.CO;2.

Wu, C.-C., K.-H. Chou, P.-H. Lin, S. D. Aberson, M. Peng, and T. Nakazawa, 2007: The impact of dropwindsonde data on typhoon track forecasts in DOTSTAR. *Wea. Forecasting*, **22**, 1157–1176, doi:10.1175/2007WAF2006062.1.

Wurman, J., D. Dowell, Y. Richardson, P. Markowski, E. Rasmussen, D. Burgess, L. Wicker, and H. B. Bluestein, 2012: The second Verification of the Origins of Rotation in Tornadoes Experiment: VORTEX2. *Bull. Amer. Meteor. Soc.*, **93**, 1147–1170, doi:10.1175/BAMS-D-11-00010.1.

Xue, M., and W. J. Martin, 2006a: A high-resolution modeling study of the 24 May 2002 dryline case during IHOP. Part I: Numerical simulation and general evolution of the dryline and convection. *Mon. Wea. Rev.*, **134**, 149–171, doi:10.1175/MWR3071.1.

——, and ——, 2006b: A high-resolution modeling study of the 24 May 2002 dryline case during IHOP. Part II: Horizontal convective rolls and convective initiation. *Mon. Wea. Rev.*, **134**, 172–191, doi:10.1175/MWR3072.1.

Yanai, M., 1964: Formation of tropical cyclones. *Rev. Geophys.*, **2**, 367–414, doi:10.1029/RG002i002p00367.

Zhu, K., Y. Pan, M. Xue, X. Wang, J. S. Whitaker, S. G. Benjamin, S. S. Weygandt, and M. Hu, 2013: A regional GSI-based ensemble Kalman filter data assimilation system for the rapid refresh configuration: Testing at reduced resolution. *Mon. Wea. Rev.*, **141**, 4118–4139, doi:10.1175/MWR-D-13-00039.1.

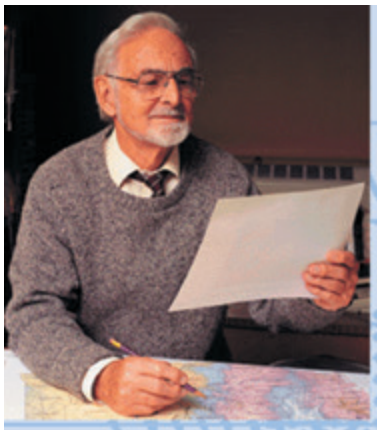

A Half Century of Progress in Meteorology: A Tribute to Richard Reed

edited by Richard H. Johnson and Robert A. Houze Jr.

with selections by: Lance F. Bosart Robert W. Burpee Anthony Hollingsworth James R. Holton Brian J. Hoskins Richard S. Lindzen John S. Perry Erik A. Rasmussen Adrian Simmons Pedro Viterbo

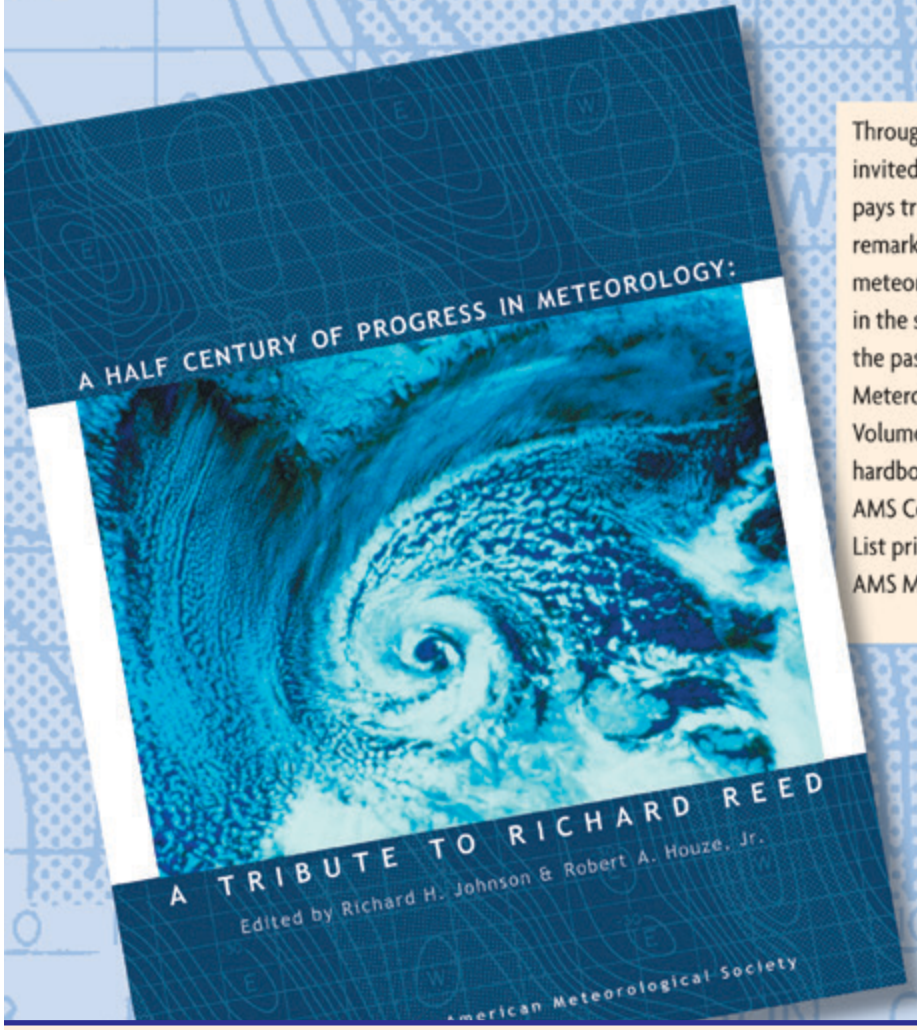

Through a series of reviews by invited experts, this monograph pays tribute to Richard Reed's remarkable contributions to meteorology and his leadership in the science community over the past 50 years. 2003. Meteorological Monograph Series, Volume 31, Number 53; 139 pages, hardbound; ISBN 1-878220-58-6; AMS Code MM53.
List price: $80.00
AMS Member price: $60.00

ORDER ONLINE: bookstore.ametsoc.org or see the order form at the back of this issue